LIFE SCIENCES

Tissue-engineered grafts exploit axon-facilitated axon regeneration and pathway protection to enable recovery after 5-cm nerve defects in pigs

Douglas H. Smith[1,2], Justin C. Burrell[1,3,4], Kevin D. Browne[1,3], Kritika S. Katiyar[1,2,3], Mindy I. Ezra[1], John L. Dutton[1], Joseph P. Morand[1], Laura A. Struzyna[1,3,4], Franco A. Laimo[1,3], H. Isaac Chen[1,3], John A. Wolf[1,3], Hilton M. Kaplan[5], Joseph M. Rosen[6], Harry C. Ledebur[2], Eric L. Zager[1], Zarina S. Ali[1,3], D. Kacy Cullen[1,2,3,4]*

Functional restoration following major peripheral nerve injury (PNI) is challenging, given slow axon growth rates and eventual regenerative pathway degradation in the absence of axons. We are developing tissue-engineered nerve grafts (TENGs) to simultaneously "bridge" missing nerve segments and "babysit" regenerative capacity by providing living axons to guide host axons and maintain the distal pathway. TENGs were biofabricated using porcine neurons and "stretch-grown" axon tracts. TENG neurons survived and elicited axon-facilitated axon regeneration to accelerate regrowth across both short (1 cm) and long (5 cm) segmental nerve defects in pigs. TENG axons also closely interacted with host Schwann cells to maintain proregenerative capacity. TENGs drove regeneration across 5-cm defects in both motor and mixed motor-sensory nerves, resulting in dense axon regeneration and electrophysiological recovery at levels similar to autograft repairs. This approach of accelerating axon regeneration while maintaining the pathway for long-distance regeneration may achieve recovery after currently unrepairable PNIs.

INTRODUCTION

Peripheral nerve injury (PNI) affects approximately 20 million people in the United States, often resulting in debilitating motor and/or sensory deficits (*1*–*4*). PNIs typically occur in the upper and lower extremities due to myriad causes, including transportation accidents, sports-related injury, combat situations, or iatrogenic incidents (*5*). Injuries where the overall nerve structure remains intact, such as crush or stretch injuries, often result in a "wait-and-see" approach to determine whether function returns spontaneously. More severe PNI cases resulting from nerve disconnection require surgical repair to reconnect the proximal and distal nerve stumps by tension-free direct anastomosis or using a biological graft or nerve conduit (*5*). However, functional recovery following PNI is generally unsatisfactory irrespective of surgical repair strategy or injury location (*6*).

Poor functional outcomes result from the inability of current repair options to overcome the long regenerative distances and times necessary to reinnervate distal targets (*7*). Slow rates of axonal regeneration (~1 mm/day) over long regenerative distances lead to prolonged denervation and, in turn, diminished regenerative capacity (*7*). Specifically, when axonal integrity is compromised, the axon segment distal to the injury site rapidly degenerates, a consequence of being disconnected from its cell body, which resides within (motor neurons) or adjacent to (sensory neurons) the spinal cord. To restore function, axon regeneration must cross not only any gap between the proximal and distal nerve stumps but also through the entire distal nerve segment to reach the end targets.

To support this process, there is a choreographed sequence of alterations in Schwann cell structure and function, where they initially assume a proregenerative phenotype to form the bands of Büngner composed of highly aligned Schwann cell columns and fibrin cables to facilitate axon regrowth. However, it is believed that this proregenerative environment degrades over several months, ultimately blunting the extent of axonal regeneration and, hence, functional recovery (*7*). This is particularly relevant in cases of long segmental defects and/or proximal injuries where this proregenerative capacity remains for a shorter time frame than necessary to support axonal regeneration to distal targets, which can take several months to years. In addition, prolonged denervation (>12 months) negatively affects target muscles and ultimately will render them irrevocably unresponsive to attempted reinnervation (*5*, *7*, *8*). Thus, a primary cause of poor functional recovery following major PNI is the gradual loss of the ability of specialized support cells and end targets to facilitate regeneration.

To date, the gold standard to bridge a nerve gap is the sensory nerve autograft. For decades, the field has tried with limited success to develop bridging solutions to replace the autograft and thus eliminate the need for harvesting healthy donor nerve, which creates an additional surgical wound site. For instance, nerve transfers are an innovative surgical technique that uses axon fascicles dissected from healthy nerves to partially restore motor functionality. In addition, a handful of devices have been commercialized [e.g., nerve guidance tubes (NGTs) such as Baxter's GEM NeuroTube, Stryker's Neuroflex, and Axogen's acellular nerve allograft (ANA; Avance)]. However, clinical use of these products is limited primarily to noncritical sensory nerve injuries close to targets (e.g., PNI in the hand or wrist), with virtually all motor and critical sensory nerves repaired using autografts. Moreover, other surgical advancements, such as

[1]Center for Brain Injury and Repair, Department of Neurosurgery, Perelman School of Medicine, University of Pennsylvania, Philadelphia, PA, USA. [2]Axonova Medical LLC, Philadelphia, PA, USA. [3]Center for Neurotrauma, Neurodegeneration and Restoration, Corporal Michael J. Crescenz Veterans Affairs Medical Center, Philadelphia, PA, USA. [4]Department of Bioengineering, School of Engineering and Applied Science, University of Pennsylvania, Philadelphia, PA, USA. [5]New Jersey Center for Biomaterials, Rutgers University, Piscataway, NJ, USA. [6]Division of Plastic Surgery, Dartmouth Hitchcock Medical Center, Dartmouth College, Lebanon, NH, USA.
*Corresponding author. Email: dkacy@pennmedicine.upenn.edu

the end-to-side coaptation, have led to "babysitting" procedures that aim to maintain the proregenerative distal pathway by redirecting axons from a nearby donor nerve to innervate distal nerve structures and muscle (*9*–*15*). Despite promise in preclinical models, clinical implementation of end-to-side transfers has been inconclusive (*10*, *12*). However, end-to-side nerve transfer not only requires an expendable donor nerve in close proximity to the distal segments of the injured nerve (which may not be available) but also typically results in a donor deficit. Often, these procedures are only used as a last resort in cases where the patient has not shown functional recovery many months following an initial PNI surgery.

These shortcomings may be addressed by tissue engineering solutions to both bridge major nerve lesions and maintain the regenerative pathway and end targets (*16*). Such tissue-engineered medical products not only would have the potential to improve outcomes but also would obviate the need to sacrifice noninjured nerves for repair procedures (*5*). The development and testing of candidate tissue-engineered solutions require valid preclinical models that adequately replicate the key challenges of clinical PNI. For instance, the length of the segmental defects tested needs to exceed the "critical nerve gap," which is approximately 4 to 5 cm in humans and other large mammals compared to 1.5 to 2 cm in small animals (*8*). Moreover, large total regenerative distances that likely require babysitting approaches (e.g., ≥20 cm, typically requires >6 months for reinnervation) are important to model, yet this is not possible in smaller animals such as rodents or rabbits. Large animal models are uniquely able to replicate the large segmental defects and long total regenerative distances necessary to capture the critical biological processes that hinder nerve regeneration in humans.

To address the major challenges in the field, we have developed tissue-engineered nerve grafts (TENGs) as an advanced regenerative strategy to reduce or obviate the need for autograft harvests (Fig. 1). TENGs are biofabricated in custom mechanobioreactors and are composed of long axon tracts spanning two neuron populations, generated via continuous mechanical tension or "stretch growth" (*17*–*21*). Axon stretch growth occurs naturally during in vivo development, such as the extension of long bones driving nerve extension. Harnessing this natural process, we have demonstrated that numerous neuronal subtypes across multiple species and ages can be induced to grow long axon fascicles in vitro (*17*, *18*, *22*–*25*). Following stretch growth, these living axon tracts are embedded in a three-dimensional (3D) extracellular matrix, rolled into a tubular form (with the axon tracts running longitudinally), and inserted within an NGT (*20*, *21*, *26*). Moreover, we recently demonstrated nerve regeneration across TENGs based on a newfound mechanism referred to as "axon-facilitated axon regeneration (AFAR)" that resulted in an accelerated regeneration and extent of electrophysiological recovery following repair of a 1-cm sciatic lesion in rats compared to repair with an NGT alone (*26*).

Building on these findings, the current study used rat and pig models of PNI to investigate the ability of TENG axons to both "babysit" the proregenerative state of host Schwann cells and to "bridge" long segmental defects (5 cm) via the newly found mechanism of AFAR. Initial babysitting studies were performed in a rat model of chronic axotomy, where we hypothesized that TENG axons would penetrate the host nerve and maintain the presence of proregenerative Schwann cells. Then, porcine TENGs were developed using embryonic sensory neurons to allow testing of allogeneic constructs in pig PNI models, where axons were "stretch grown" to form TENGs spanning 5 cm in a remarkably short time frame of 2 to 3 weeks. We hypothesized that TENGs would serve as a living scaffold to guide sprouting axons from the host proximal nerve stump across the nerve lesion and into the distal nerve stump. Initial porcine studies evaluated TENG neuronal survival, mechanism of action (i.e., AFAR), and efficacy following 1- and 5-cm lesions in the deep peroneal nerve (DPN; ~20 cm from muscle end targets). Last, we showed that TENGs facilitated reinnervation and electrophysiological recovery when used to bridge 5-cm segmental defects in the common peroneal nerve (CPN; ~27 cm from distal muscle end targets), with or without the use of secondary babysitting TENG implants. Collectively, our findings demonstrate the efficacy of large-scale TENGs in challenging, clinically relevant porcine models featuring both large segmental defects (5 cm) and long total regenerative distances to reach distal targets (20 or 27 cm).

RESULTS

TENG transplants into the distal nerve segment maintain proregenerative Schwann cells in a model of chronic axotomy in rats

We hypothesized that chronic interactions between transplanted axons and host Schwann cells would maintain the proregenerative efficacy of host Schwann cells in an otherwise axotomized nerve, thus increasing the regenerative capacity for ultralong-distance nerve regeneration. To test this hypothesis, we created a chronic axotomy model in rats by transecting the sciatic nerve, capping the proximal stump to prevent host axon growth, and implanting an NGT (negative control) or living stretch-grown TENG spanning 1 cm sutured to the distal stump. We performed histological analyses up to 16 weeks after transection to determine distal nerve cytoarchitecture, graft survival, and graft axon integration with distal nerve (Fig. 2A).

In this model, TENG neurons were found in the proximal and distal regions of the graft, as expected on the basis of the transplantation and encapsulation paradigm, with robust axonal extension that integrated with the host tissue (Fig. 2B). Schwann cell morphology in the distal nerve was assessed by comparing $S100^+$ expression. Over 2 to 4 weeks after transection, distal nerve Schwann cells formed stereotypically aligned regenerative columns. In control animals (not receiving TENGs), the density of these columns decreased over 6 to 8 weeks, with a marked reduction in Schwann cell presence and alignment after 9 weeks and widespread loss of Schwann cells and a complete absence of alignment by 16 weeks (Fig. 2C). In contrast, in animals receiving TENGs, an abundance of $S100^+$ Schwann cells were observed up to at least 16 weeks, suggesting that TENGs may preserve the proregenerated state in distal nerve Schwann cells in this model of chronic axotomy ($P < 0.001$; Fig. 2D). Moreover, this effect of Schwann cell preservation in animals receiving TENG implants was observed at least 3.0 cm away (the furthest distance assessed) from the implantation sites in far distal nerve branches, demonstrating a considerable spatial effect of graft axonal projections (Fig. 2E). In addition, even a sparse distribution of TENG axons was shown to maintain Schwann cells across an entire fascicle, suggesting a considerable amplification effect (Fig. 2F). The procedure to cap the proximal nerve was effective in all cases, as potentially aberrant regeneration of the proximal stump into the distal pathway was not observed in any of the animals. This demonstrated the efficacy of axons projecting from stretch-grown TENGs to babysit otherwise axotomized Schwann cells in the distal nerve sheath to maintain

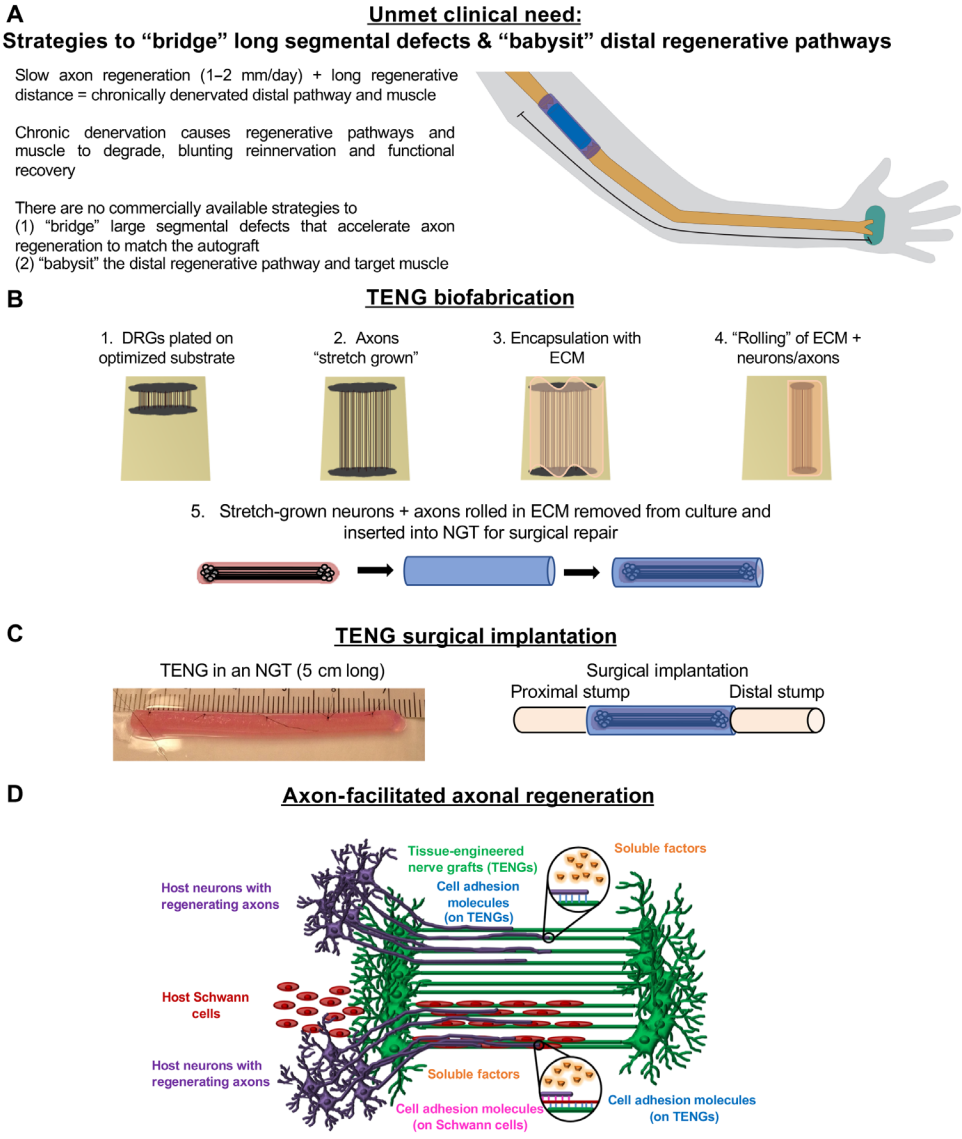

Fig. 1. Overview of clinical need and tissue-engineered solution. (**A**) Clinical unmet need requires bridging + babysitting strategy. Functional recovery after PNI is often limited because of chronic denervation of the distal pathway resulting from slow axon regeneration across ultralong regenerative distances to muscle end targets. Although current repair strategies aim to accelerate regeneration, none of the commercially available approaches are designed to mitigate complications associated with chronic denervation. (**B**) TENG biofabrication. We have bioengineered stretch-grown axons from (1) embryonic rat or pig sensory DRG neurons that are cultured on two overlapping membranes in a custom-built mechanobioreactor, allowing for integration between the two populations for up to 5 DIV. (2) The two overlapping membranes are gradually separated via a microstepper motor to apply mechanical tension to the axons spanning the two neuronal populations, depending on the desired length. (3) Stretch growth occurs for days to weeks at 1 to 10 mm/day. Once the desired axon length is reached, the neurons and stretch-grown axons are encapsulated in collagen extracellular matrix (ECM) for stabilization. (4) Encapsulated constructs are "rolled" and (5) inserted into an NGT or nerve wrap to bridge segmental nerve defects. (**C**) TENG surgical implementation. Example of a 5-cm TENG-NGT and schematic of surgical implementation. (**D**) TENG proregenerative mechanism of action. Concept figure illustrating the dual mechanisms of TENG-mediated regeneration [as described in detail in the work of Katiyar *et al.* (*25*)] via AFAR whereby host axons rapidly grow directly along TENG axons, as well as host Schwann cells (SCs) migrating directly along TENG axons to efficiently fill the length of the graft zone.

their presence and proregenerative capacity out to at least several centimeters from the implant site.

TENGs were biofabricated, composed of stretch-grown axons from porcine neurons

To test allogeneic TENGs in porcine models of PNI, we first needed to generate TENGs using porcine neurons via our previously described process of axon growth via continuous mechanical tension or stretch growth (*17*, *26*). For these studies, dorsal root ganglia (DRG) sensory neurons were isolated from fetal pigs and were cultured within custom-built mechanobioreactors (Fig. 3). These neuron cultures were subjected to axonal stretch growth to create constructs consisting of living, aligned axonal tracts grown to lengths of 0.5 to 5.0 cm (Fig. 3, E to H). In vitro, we characterized TENG structure and function based on our established quality control metrics involving DRG count, neuron health, axon structure, and

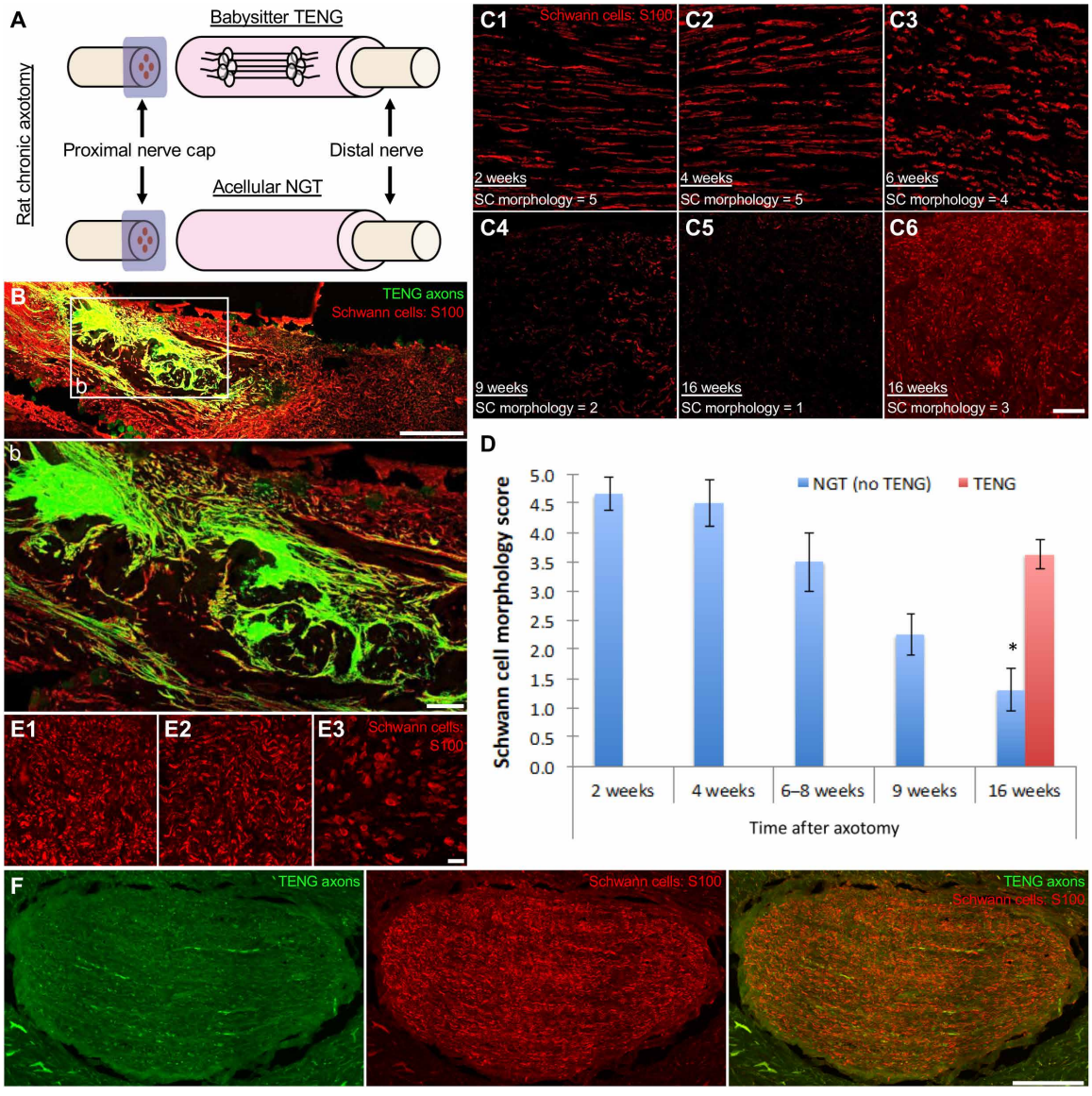

Fig. 2. Implanted TENGs integrate with denervated distal nerve sheath over 16 weeks in rodent chronic axotomy model. (**A**) Proregenerative S100$^+$ SCs were characterized in a rodent chronic axotomy model by securing to the otherwise denervated distal nerve with either a babysitting TENG or empty NGT (negative control). See Fig. 1B for additional information on encapsulation methodology. (**B**) Longitudinal tissue sections showing dense TENG neurons (predominantly showing the cell body region of the graft) transduced to express GFP survive transplantation and project axons into the otherwise denervated distal nerve stump. (b) Higher magnification revealed TENG axons growing in close proximity to host SCs. (**C1** to **C5**) Following NGT implant alone, host SCs initially formed stereotypically aligned regenerative columns at 2 and 4 weeks but become disorganized over 6 to 9 weeks and disappear virtually completely by 16 weeks, suggesting a nonpermissive regenerative environment. (**C6**) In contrast, distal SCs were preserved in animals receiving TENGs at 16 weeks. (**D**) Semiquantitative scoring of SC presence and morphology revealed that TENGs preserve SCs in the otherwise axotomized distal nerve structure for prolonged time periods. (**E1** to **E3**) Aligned SCs were found at 16 weeks after axotomy, distal to the babysitting TENG (E1) 0.2 cm, (E2) 1.0 cm, and (E3) 3.0 cm from the graft. (**F**) Oblique (45°) section of the distal nerve showing that GFP$^+$ axons projecting from the babysitting TENG persist within the distal nerve stump at 16 weeks after transplantation, closely interacting with host SCs. Here, a relatively low "dose" of TENG axons may babysit an entire fascicle of host SCs. *P* values are represented as $*P < 0.001$. Scale bars, 250 μm and 50 μm (B and b), 50 μm (C), 20 μm (E), and 25 μm (F). $n = 3$ to 4 for NGT per time point; $n = 4$ for babysitting TENG at 16 weeks.

axon density. These analyses have occurred within our custom mechanobioreactors after stretch, as well as following proteinaceous encapsulation and removal from the mechanobioreactors. Here, porcine TENGs were found to be healthy, with densely fasciculated (i.e., bundled) axon tracts. After stretch, porcine TENGs were subsequently created by embedding these living axon tracts in a 3D matrix and removing them en masse for transplantation (Fig. 3I).

Porcine TENGs exploit AFAR to facilitate host axon regeneration and Schwann cell infiltration across short segmental defects in motor and sensory nerves

We next assessed acute repair in 1.0-cm lesions in the sensory (sDPN) and motor (mDPN) branches of the DPN in a swine model of PNI as a stepping stone to chronic repair of 5.0-cm lesions in the DPN (Fig. 4A). Our objectives in this study were to assess TENG survival

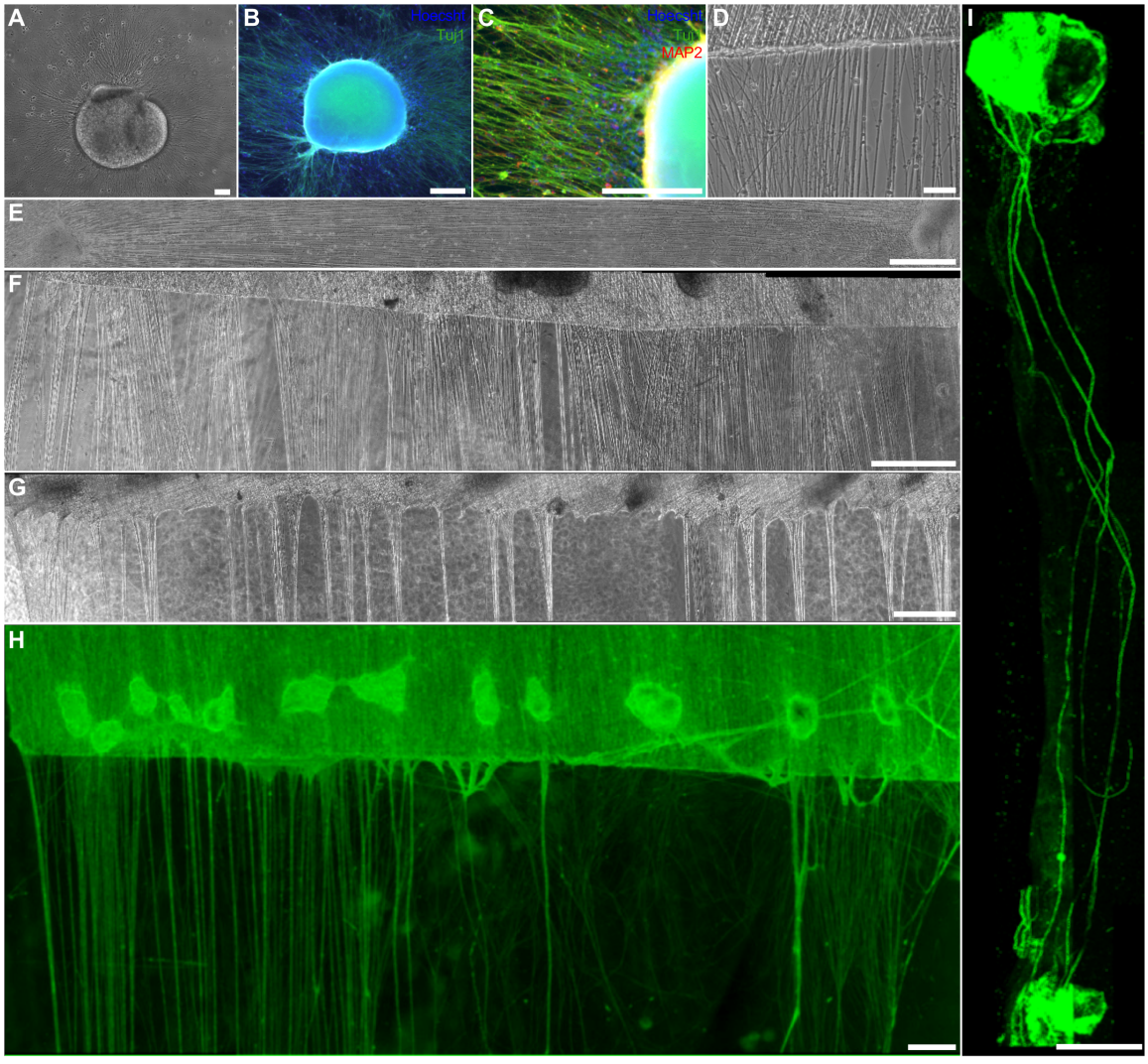

Fig. 3. Primary porcine neurons subjected to axonal stretch growth to biofabricate TENGs. E40 transgenic GFP$^+$ porcine DRG neuron cultures (**A**) at 1 DIV in phase contrast and (**B** and **C**) at 7 DIV with fluorescent microscopy labeling nuclei (Hoechst), axons (Tuj1), and neuronal cell bodies and dendrites (MAP2). (**D**) Axons from porcine neurons extend beyond the towing membrane to integrate with the other neuron population on the base membrane. Aligned axon tracts are generated following mechanical stretch growth, as shown in phase-contrast microscopy. (**E**) Example of DRG populations that were stretch-grown over 1 cm shown with phase-contrast microscopy. (**F**) Phase-contrast image of the towing membrane side of a TENG showing healthy and robust axons. (**G** and **H**) Examples of a 5-cm-long TENG with dense fasciculation following stretch growth at 21 DIV (5 days before stretch, 16 days of stretch growth), shown in (G) phase contrast and with (H) fluorescent (GFP) microscopy. (**I**) Example of a 2.5-cm-long GFP$^+$ TENG following collagen encapsulation before transplantation. Scale bars, 100 μm (A), 500 μm (B and C), 50 μm (D), 1000 μm (E), 100 μm (F), 1000 μm (G and H), and 2.0 mm (I).

in a large animal model, investigate whether TENGs influence host regeneration, and compare acute regeneration metrics to autografts and NGTs alone. Our hypothesis was that TENG neurons and axons would serve as a living scaffold to guide sprouting axons from the host proximal nerve stump across the nerve lesion. To assess the regenerative response that occurred in pigs repaired with 1.0-cm TENGs, graft zones were harvested 2 weeks after implantation and immunohistochemical examination was performed on longitudinal tissue sections. Microscopic examination of tissue sections revealed surviving transplanted green fluorescent protein–positive (GFP$^+$) DRGs and maintenance of the aligned axonal architecture within all TENG transplants (Fig. 4, B to E). To assess the rates of host axon regeneration and Schwann cell infiltration, sections were stained for neurofilament protein to mark host versus TENG (GFP$^+$) axons and S100 protein to mark host Schwann cells. Robust host axon outgrowth was visualized at 2 weeks across the entire 1-cm repair zone for animals treated with TENG (Fig. 4D and figs. S2 and S3) or autograft compared to sparse regeneration following NGT repairs, demonstrating that both TENGs and autografts accelerated axon regeneration compared to NGTs alone. This provided evidence that TENGs were actively facilitating axon regeneration rather than simply behaving as a permissive substrate. Using high-resolution confocal microscopy, we directly visualized axon regeneration via the AFAR mechanism at the microscale (i.e., cell-axon and axon-axon interactions; Fig. 4, F to H). This analysis determined that regenerating axons have an intrinsic preference to grow directly along TENG

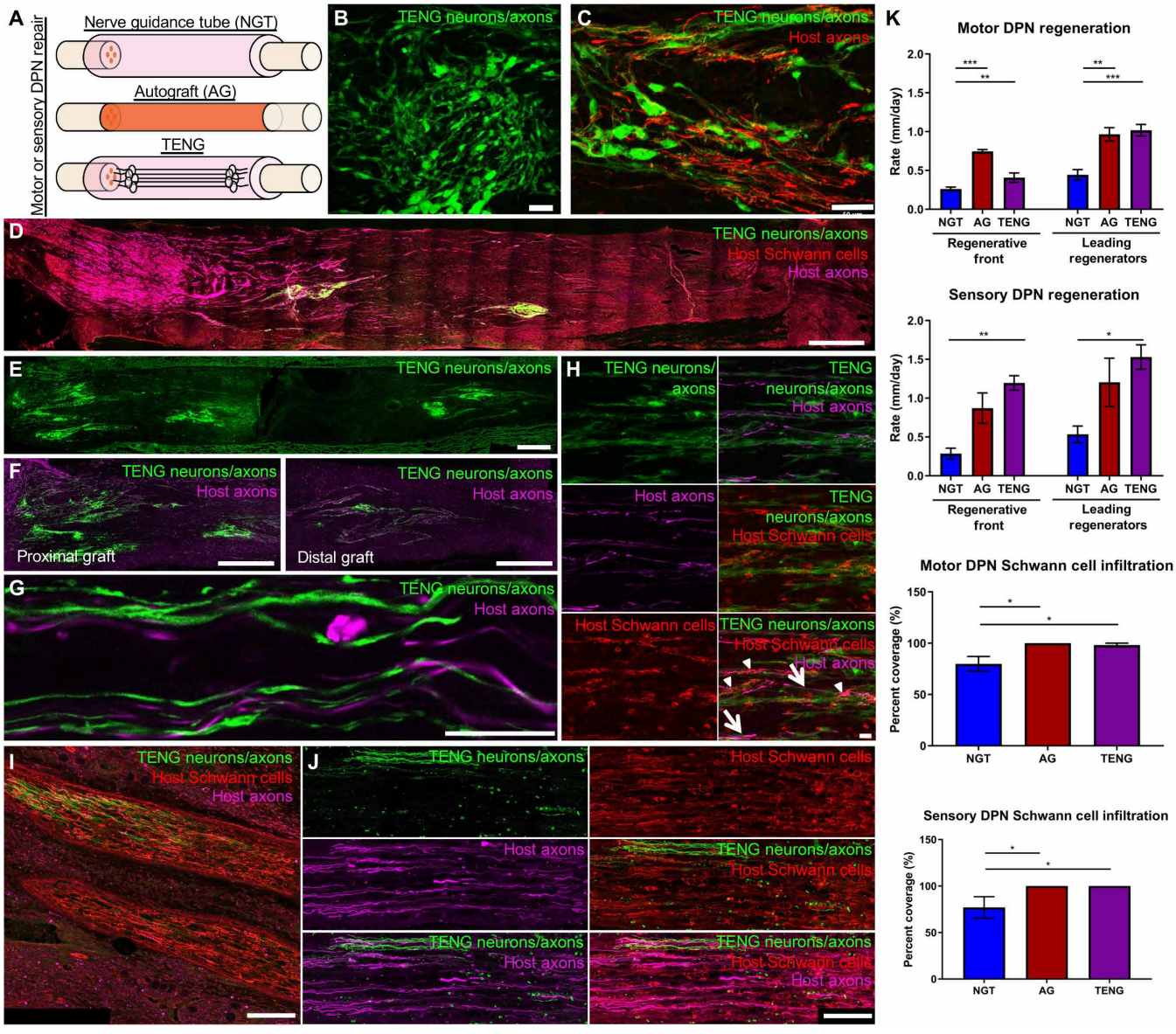

Fig. 4. TENGs maintain neuronal-axonal architecture and project axons into the host distal nerve that closely interact with host SCs and regenerating axons following a 1-cm porcine nerve repair. (**A**) Acute regenerative mechanisms of action were evaluated at 2 weeks following a 1-cm repair of the mDPN and sDPN using an NGT, autograft (AG), or TENG. (**B**) Allogeneic TENG neurons (GFP^+) survived transplantation in the absence of immunosuppression. (**C**) Robust axonal regeneration ($SMI31/32^+$) was observed along TENG neurons/axons. (**D**) Host SC infiltration ($S100^+$) and axon regeneration were visualized. (**E**) Within the graft, TENG neurons were located on both ends spanned by long-projecting axons, and (**F**) host axons were seen regenerating along TENG axons. (**G**) At higher magnification, AFAR was observed. (**H**) TENGs facilitated nerve regeneration using traditional SC-mediated axonal regeneration and also in the absence of SCs via AFAR mechanism (arrows). Host SCs aligned with TENG axons and likely support host axon regeneration (arrowheads). (**I**) Longitudinal section of the distal nerve showing columnar SCs or bands of Büngner and TENG axons. (**J**) Higher magnification revealed leading regenerator host axons within bands of Büngner in the distal nerve. (**K**) Accelerated regeneration was observed at 2 weeks following TENG repair compared to NGTs. Greater SC infiltration was also found in TENGs compared to NGTs for both nerves. No statistical differences were found for axon regeneration or SC presence between TENG and AGs. *P* values are presented as $*P < 0.05$, $**P < 0.01$, and $***P < 0.001$ versus NGT. Scale bars, 50 μm (B and C), 1000 μm (D), 500 μm (E and F), 20 μm (G and H), 250 μm (I), and 100 μm (J). For the sDPN study, $n = 4$ for autograft, $n = 4$ for NGT, and $n = 5$ for TENG. For the mDPN study, $n = 4$ for all groups.

axons, thus directly facilitating host axon regeneration. TENG axons intrinsically promote host axon growth along their structure based on this newfound mechanism, matching our recent report in a rat model of PNI (*26*).

In the evaluation of the axon regeneration process, we observed two distinct characteristics in regeneration in pigs that mirror our observations in rats: (i) a major bolus of regenerating axons ("regenerative front") and (ii) a smaller group of axons rapidly regenerating across the graft ("leading regenerator" axons). Notably, leading regenerator axons were found all the way in the distal nerve by 2 weeks following repair with TENGs and autografts but not with NGTs alone (Fig. 4, I to J). Similar to the natural developmental process of the nervous system, these TENG axons may serve as "pioneer" axons to prescribe the initial path for subsequent regenerating axons

to follow (*27*–*29*). The axon regeneration distances and rates were quantified for the regenerative front and leading regenerators for all experimental groups, demonstrating that the rate of host leading regenerators across the lesion was equivalent for animals treated with TENGs and autografts and that this rate was superior (1.6 to 4.2 times faster) compared to animals treated with NGTs alone (Fig. 4K). In general, axon regeneration progressed more slowly following repair of a predominantly motor nerve versus a predominantly sensory nerve. However, TENG-mediated repair was the only group that progressed at maximum rates of greater than 1 mm/day across the graft site for both types of nerves.

To better understand the effects that TENGs had on the nerve regeneration process, we examined the interactions of TENGs and Schwann cells, as Schwann cells are an essential component to the natural nerve regeneration process. In this study, the infiltration or migration distance of Schwann cells from the host tissue, both proximally and distally, into the TENGs and NGTs was measured. Results showed that Schwann cell infiltration distance was enhanced in animals treated with TENGs compared to NGTs alone ($P < 0.01$; Fig. 4K). Animals who received NGTs alone showed modest Schwann cell penetration from both the proximal and distal ends, with a clear Schwann cell–free gap in the center at this time point in most cases. As expected, a homogenous distribution of Schwann cells was observed within autografts. Thus, similar to the findings with host axon regrowth, we observed that Schwann cells had a strong preference to migrate directly along TENG neurons and axons, indicating that the TENGs actively influenced and directed Schwann cell infiltration. Together, these findings suggest that TENGs play an active role in accelerating the natural regeneration process by encouraging Schwann cell infiltration and alignment.

TENGs facilitate acute regeneration and chronic electrophysiological recovery when used to repair 5-cm lesions in the mDPN

On the basis of the unique mechanisms of action demonstrated in the 1-cm repair model, we hypothesized that TENGs would effectively drive regenerating axons across a challenging, clinically relevant 5-cm motor nerve repair and thereby enable electrophysiological recovery following chronic axotomy. To assess the regenerative response that occurred in animals treated with 5-cm TENGs (Fig. 5A), graft zones and distal nerve were harvested and immunohistochemical examination was performed on longitudinal and axial tissue sections. On the basis of GFP expression, microscopic examination of tissue sections revealed evidence of surviving transplanted porcine DRGs and maintenance of the aligned axonal architecture within all TENG transplants at 1 month after transplant (Fig. 5, B to H). Note that the lack of tissue at the center of the longitudinal section is not a "dead zone" in the graft; rather, it is an artifact resulting from the technical challenge of obtaining a complete 5-cm longitudinal section showing both proximal and distal ingrowth, as well as TENG neurons/axons, which are often found closer to the edges of the conduit. At this early time point, TENG axons appeared to directly facilitate host axon regeneration, and leading regenerator axons were observed penetrating the distal nerve. These host leading regenerator axons had crossed the gap to enter the distal nerve before host Schwann cells had fully infiltrated the entire 5-cm nerve repair zone (Fig. 5, C to H). This finding indicates that TENGs had facilitated axon regeneration across the lesion independent of Schwann cells, supporting observations made in the 1-cm lesion repair.

Nerve regeneration and electrophysiological function were also assessed at 3 months following TENG-mediated repair of a 5-cm lesion of the mDPN in pigs. The collagen NGT had dissolved by this time point, and the gross nerve structure appeared similar to native nerve, which was notable given that 5 cm of nerve had been completely removed (Fig. 5I). This indicates that TENGs may have facilitated the reformation of complex 3D nerve tissue. Surviving TENG neurons/axons were observed in the graft zone, and TENG axons were found penetrating into the distal nerve (Fig. 5, J, K and L). In addition, by this time point, axon regeneration and Schwann cell infiltration had occurred across the entire 5-cm repair site (Fig. 5M). Reliable compound nerve action potentials (CNAPs) were observed across nerves repaired with TENGs, indicating significant axon regeneration across the lesion and into the distal nerve at this relatively early time point (Fig. 5O). Multiple fascicles containing both host axons and TENG axons were observed in the distal nerve structure (Fig. 5N). Host axons were found to be present as far distally as was examined (9.5 cm from the proximal transection site). Although conduction of the repaired nerve was verified at this time point, nerve stimulation did not elicit a motor response (i.e., a "hoof twitch"), indicating that although axons had crossed the graft zone, axons did not yet reach the distal muscle and/or form functional neuromuscular junctions. Collectively, these results show that TENGs supported axon regeneration across a long-gap 5-cm lesion by 3 months after repair.

Nerve regeneration and electrophysiological function were next evaluated at chronic time points following bridging of 5-cm segmental defects in the mDPN (Fig. 6A). As early as 7 months after repair, electrical stimulation of the repaired nerve (proximal or distal to the repair zone) elicited an evoked motor response manifesting as a hoof twitch. Although this suggested that axon regeneration had progressed to the target muscle, the supramaximal stimulation intensity necessary to elicit an evoked muscle response was relatively high compared to the contralateral side, suggesting a nascent, immature recovery. Histologically, we then investigated the repaired nerves immediately proximal to the target muscle, revealing regenerated host axons spreading on the muscle surface by 7 months (Fig. 6, B and C). These findings demonstrated that TENG repair of 5-cm nerve lesions in the mDPN (~20 cm from the target muscle) led to axon regeneration in the immediate vicinity of the target muscle based on the evoked electrophysiological response.

By 9 months after repair, the gross architecture of the graft region appeared virtually identical to that of the adjacent uninjured nerve, suggesting significant regrowth of host nerve tissue (Fig. 6E). Cross-sectional analyses of the distal nerve structure at 9 months after repair revealed numerous fascicles containing both host and TENG axons (Fig. 6F). Notably, the fascicular architecture distal to the 5-cm TENG repair resembled uninjured nerve (see fig. S1) and included large-diameter, myelinated host axons throughout the entire distal nerve. Here, similar axon density and myelination levels were observed distal to the graft region following TENG or autograft repair (Fig. 6G). In addition, while no significant differences were found between groups for the *g*-ratio, the myelinated axon fiber distribution for the autograft group was shifted rightward compared to the TENG group, suggesting a similar degree of myelination but a greater number of large-caliber axons distal to the autograft repair (fig. S4). By 10 to 11 months, the supramaximal intensity necessary for an evoked muscle response was more physiologically normal (i.e., within the range used to stimulate a naïve nerve), indicating

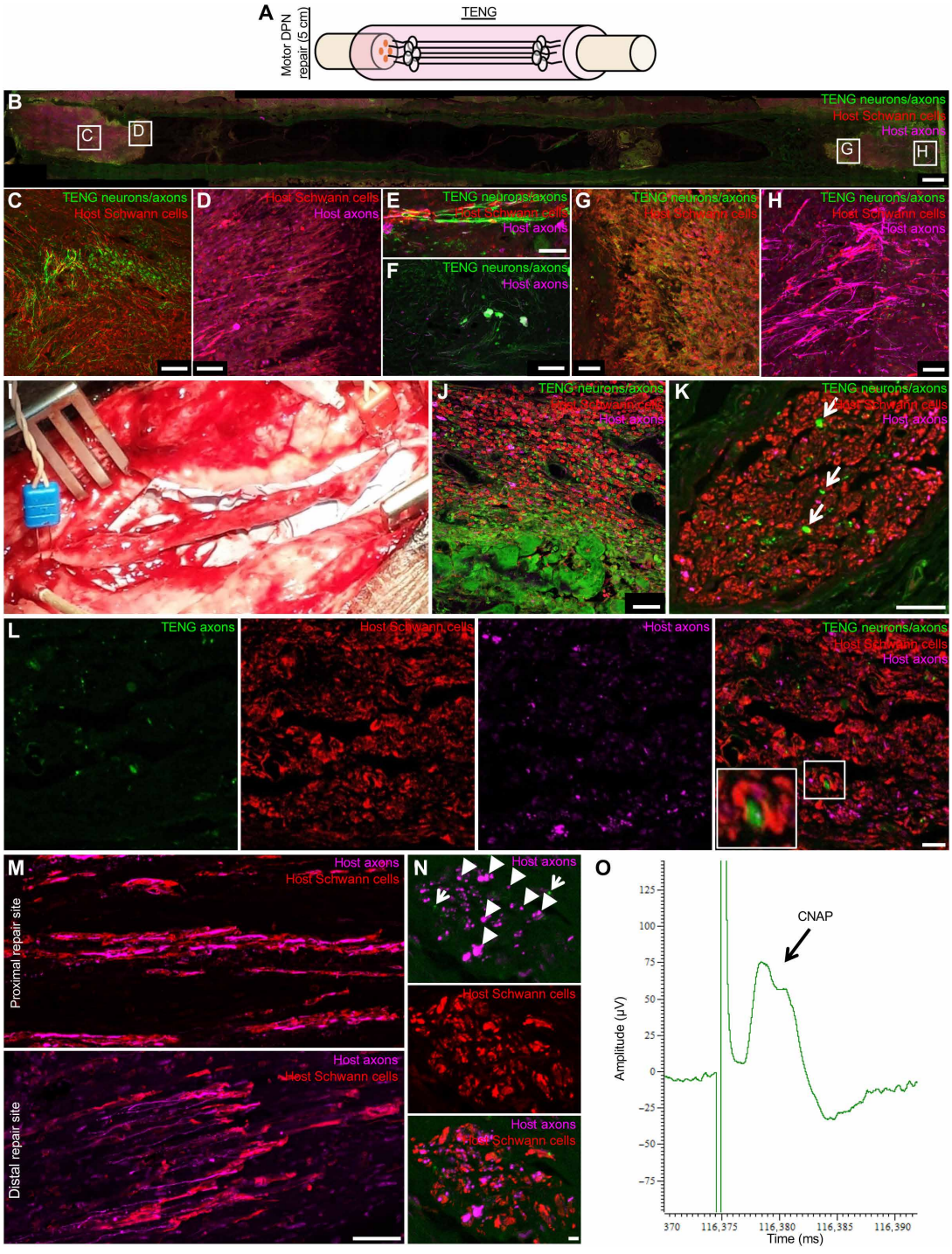

Fig. 5. Nerve regeneration at 1 and 3 months following repair of long-gap (5-cm) nerve injury with TENGs in a porcine model. (**A**) TENG efficacy was further assessed following a 5-cm mDPN repair. (**B** to **H**) At 4 weeks after repair, (B) the main bolus of regenerating axons (SMI31/32$^+$, left) and SC infiltration (S100$^+$) was visualized within the conduit (autofluorescing green). In this section, TENG neurons can be visualized in the proximal and distal conduit with some TENG axons in the center of the conduit, suggesting that the TENG axons span the entire length of the graft region. (C) Surviving TENG neurons/axons (GFP$^+$) interacted with host SCs. (D) Dense host axon regenerative front and host SCs were found penetrating the graft. (E) Notably, host axons and aligned SCs grew along TENG axons near the conduit center. (F) TENG neurons/axons and (G) infiltrating host SCs were visualized within the graft. (H) Host axons were visualized in the distal nerve before complete SC infiltration, further suggesting that TENGs facilitated axon regeneration independent of SC infiltration. (**I** to **O**) At 12 weeks, (I) gross nerve structure shows the reformation of nerve and vascular tissue. (J) Surviving TENG neurons/axons interacted with host SCs. (K and L) Axial sections distal to the graft show (K) successful host axon regeneration and TENG axon penetration distally and (L) the presence of TENG axons, host SCs, and host axons at higher magnification. (M) Successful host axon regeneration and SC infiltration near both ends of the 5-cm graft. (N) Large-caliber host axons (arrowheads) and smaller-caliber TENG axons (arrows) were observed in the distal nerve. (O) CNAPs following TENG repair indicate significant axonal regeneration. Scale bars, 1000 μm (B), 100 μm (C), 50 μm (D to H, J, K, and M), 15 μm (L), and 5 μm (N).

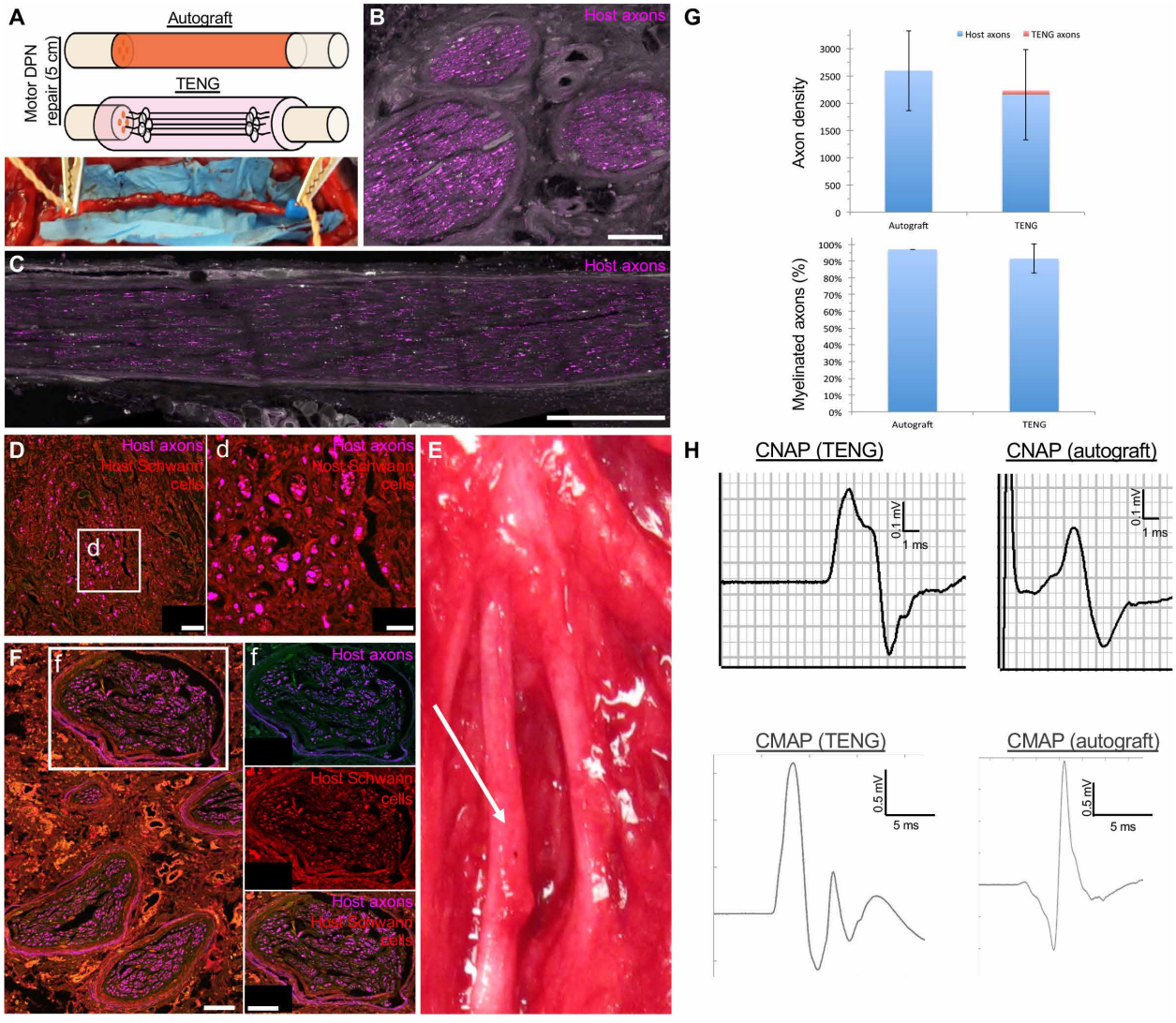

Fig. 6. Axon regeneration and muscle reinnervation following a 5-cm segmental repair of the mDPN in swine. (**A**) At 7 months following TENG repair, the regenerated mDPN was isolated from the surrounding tissue for functional assessment. (**B**) Oblique nerve section from the extreme distal mDPN directly at the interface with the target muscle indicates that host axons (SMI31/32^{+}) had reached the muscle by 7 months after repair. (**C**) Same nerve as (B) showing longitudinal nerve section from a more proximal zone. (**D**) Cross-sectional immunohistochemistry of the mDPN 5 mm distal to the TENG was performed to label host axons and SCs. (d) Higher magnification revealed a high density of host axons in the distal nerve surrounded by S100^{+} SCs. (**E**) At 9 months after repair with a TENG (arrow), the nerve gross structure and morphometry appeared indistinguishable from those of an adjacent, nonrepaired nerve. (**F**) Nerve morphometry showed fasciculation, dense axonal regeneration, and remyelination following TENG repair at 9 months after repair (5 mm distal to the repair zone). (f) Higher magnification of an individual fascicle revealed large- and small-diameter host axons surrounded by SCs, potentially indicating ongoing maturation. (**G**) Morphometric analysis revealed that axon density and percentage of myelinated axons were equivalent between animals repaired with a TENG or a sensory autograft (see fig. S4 for breakout of myelinated axon and *g*-ratio profiles). (**H**) An evoked hoof twitch was consistently achieved by 7 months after repair with robust CNAP and CMAPs, further suggesting successful axon regeneration, myelination, and muscle reinnervation. No significant differences were found ($P > 0.05$). Scale bars, 50 μm (B), 500 μm (C), 50 μm (D), 20 μm (d), and 50 μm (F and f). $n = 3$ for autografts and $n = 5$ for TENGs at this time point.

mature axonal regeneration, myelination, and muscle recovery. Nerve stimulation resulted in robust and reproducible CNAPs and compound muscle action potentials (CMAPs; Fig. 6H). CNAPs and CMAPs were observed across the nerve graft, with a comparable percent recovery between the repair of 5-cm lesions using TENG and autograft (typically 40 to 60% of the contralateral CMAP level was achieved).

Babysitting TENGs integrate with the distal nerve to promote axon regeneration and electrophysiological recovery following primary repair of 5-cm segmental defects in the CPN

On the basis of the previous findings demonstrating that TENG axons preserve host Schwann cells in models of chronic axotomy and that TENGs facilitate electrophysiological recovery across long segmental defects, we postulated that axon outgrowth extending from babysitting

TENGs would maintain the proregenerative environment of the distal segment as the host axons regenerate across the long gap. To evaluate the proregenerative efficacy of TENGs following chronic denervation (i.e., due to long regenerative distance), regeneration and electrophysiological recovery were assessed in a challenging, clinically relevant model featuring a 5-cm segmental defect in the CPN repaired with a long "bridging" TENG and with or without two babysitting TENGs implanted in-line in the mDPN (Fig. 7A). At 12 months following a 5-cm TENG primary repair and simultaneous transplantation of distal babysitting TENGs in the mDPN,

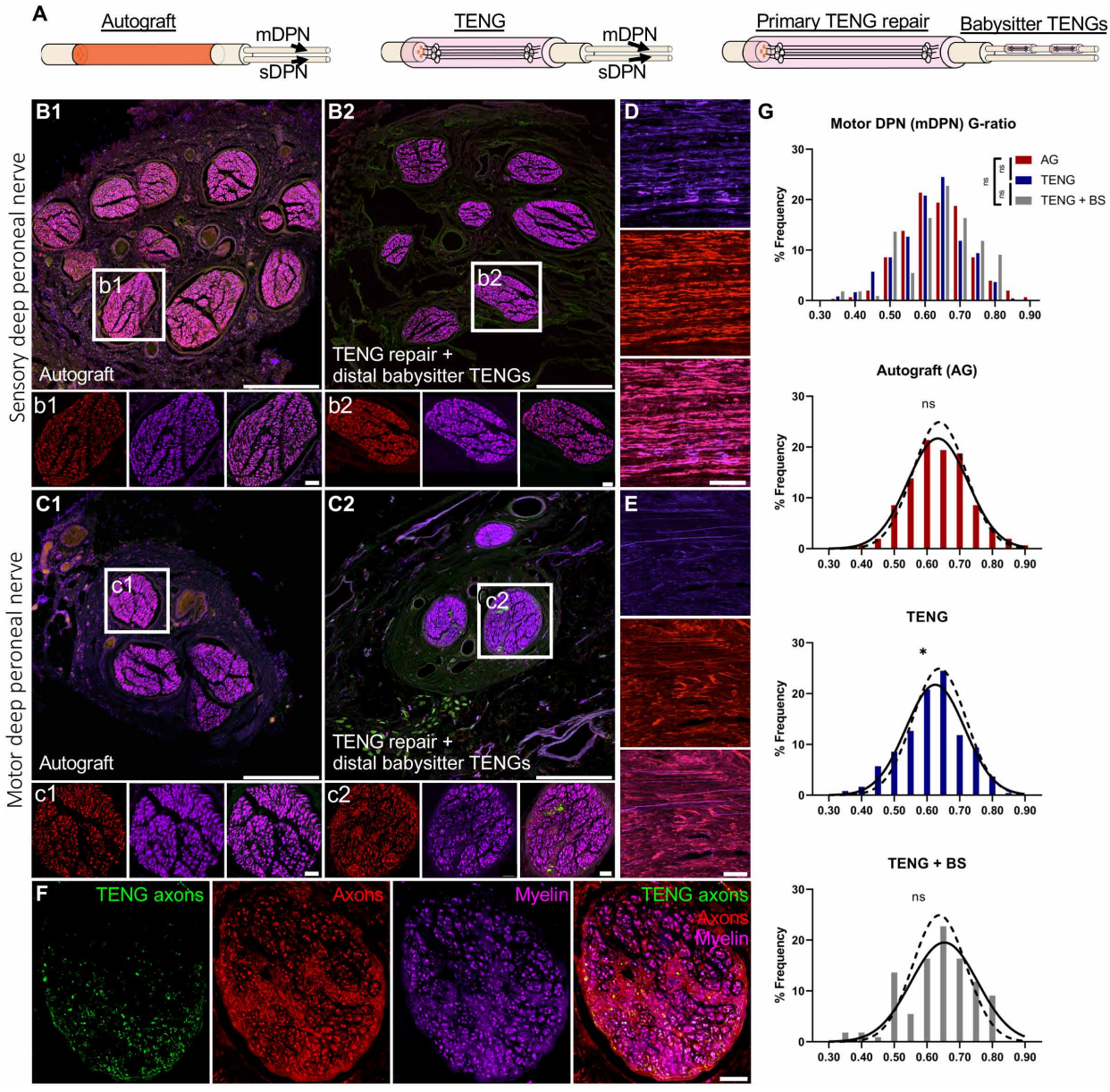

Fig. 7. Deployment of distal TENGs to babysit the distal pathway following repair of 5-cm segmental defects in the CPN in swine. (**A**) To evaluate the efficacy of simultaneously reconstructing proximal injuries (bridge) and preserving the distal nerve and motor targets (babysit), two babysitting TENGs were placed in continuity with the mDPN, distal to the primary CPN repair. (**B** and **C**) Immunohistochemistry distal to the primary CPN graft revealed axon regeneration and maturation in the (B) sDPN and (C) mDPN at 12 months following autograft or TENG repair with distal babysitting TENGs in the mDPN. (C2) GFP^+ signal was found within the mDPN fascicles at 12 months following primary TENG repair and transplantation of distal babysitting TENGs. (**D** and **E**) Longitudinal sections showing host axons and aligned SCs present in the (D) sDPN and (E) mDPN at the babysitting graft zone, several centimeters distal to the primary CPN repair, further corroborating that host axons crossed the babysitting TENG. (**F**) High magnification of an mDPN fascicle revealed numerous TENG axons that closely interact with host SCs. (**G**) Detailed histological analysis revealed that *g*-ratio distribution profiles in the mDPN were similar across groups at this time point. Individual *g*-ratio distribution profiles were broken out and compared to the naïve contralateral nerve distribution (dotted line). No significant differences were found for the mDPN *g*-ratio distribution profiles between the groups or between the contralateral (naïve) mDPN nerve and the mDPN nerve distal to the autograft or TENG + BS repair at this time point. *G*-ratio distributions were compared between groups for each nerve using the two-sample Kolmogorov-Smirnov test. *P* values are represented as $*P < 0.05$. See figs. S5 and S6 for breakout of myelinated axon and *g*-ratio profiles. Scale bars, 500 μm (B and C) and 50 μm (b and c). At least $n = 100$ axons were measured per animal. ns, not significant.

host axons regenerated across the 5-cm defect into the distal branches (Fig. 7, B and C). TENG axons were found in the mDPN distal to the babysitting TENGs, likely integrating with otherwise axotomized host Schwann cells and muscle months ahead of the regenerating host axons extending from the proximal nerve stump (Fig. 7). Detailed analysis revealed that the density of TENG axons from babysitting grafts was proportional to the density of regenerating host axons ($R^2 = 0.78$). Moreover, a greater density of babysitting TENG axons corresponded with a modest increase in the diameter in host axons, suggesting that babysat fascicles may allow for more rapid host axon maturation. With respect to axon maturation, there were no significant differences in the *g*-ratio of the mDPN branch 5 mm distal to its bifurcation between the groups and no significant difference between the contralateral mDPN and the autograft or TENG + distal babysitting TENG (BS) groups (Fig. 7G). Detailed breakouts of the myelinated axon and *g*-ratio distribution profiles for the CPN, mDPN, and sDPN suggest varying degrees of maturation for each nerve based on repair strategy (figs. S5 and S6).

In addition, regenerated host axons were quantified in the CPN distal to the primary graft region and in the distal sDPN and mDPN branches at 12 months after repair (Fig. 8, B to D). Although a greater number of axons were found in the distal CPN following TENG repair compared to autograft repair, no significant differences were found in the distal branches (Fig. 8E). Moreover, the maturation of the regenerated axons, based on *g*-ratio and myelinated axon diameter, was similar across treatment groups, with only subtle differences found (figs. S5 and S6). For all repair strategies assessed, the histological findings were corroborated via positive electrophysiological recordings at 9 and 12 months (Fig. 8F). In all cases, a robust evoked muscle response was observed from the tibialis anterior before any positive response from the distal extensor digitorum brevis (EDB). Moreover, a more robust signal was observed at 12 months as compared to 9 months, indicating an ongoing maturation and recovery response. Notably, evoked CMAP recordings with corresponding hoof twitch were obtained following CPN repair using a 5-cm TENG primary graft and distal babysitting TENG grafts, indicating successful nerve regeneration and muscle innervation in this novel dual bridging-babysitting paradigm.

DISCUSSION

Here, we used a stepwise approach to evaluate dual strategies of transplanting TENGs to both bridge nerve gaps and babysit the distal nerve pathway to promote long-distance regeneration and recovery of electrophysiological function. Specifically, using different models of PNI, from a chronic axotomy model in the rat to a clinically relevant 5-cm lesion in swine, we demonstrated that TENG axons support or babysit host Schwann cells in distal nerve sheaths that were devoid of host axons. In addition, in swine models, we demonstrated that the transplanted TENG axons served as a living pathway to facilitate host axon regeneration across the lesion and all the way to the end targets. Last, we demonstrated that TENG repair restored the electrophysiological function of the nerve to target muscle(s) far beyond the injury site.

Despite advancements in peripheral nerve surgery, two critical challenges continue to limit successful regeneration and functional recovery: graft length and total regenerative distance to end target. For example, disconnection of brachial plexus nerves requires growth of axons down the entire length of the arm. Limited functional recovery results from prolonged denervation due to these long regenerative distances and slow axonal regeneration (1 to 2 mm/day). Successful regeneration is further diminished following the eventual degradation of the proregenerative Schwann cell formations in the distal nerve, described as the bands of Büngner (*7*). Moreover, severe cases of PNI, such as segmental nerve injury, result in the loss of many supportive cells necessary to guide axon outgrowth. Several bridging strategies are currently in clinical use, including nerve autograft (which requires harvest of an intact functional donor nerve with potential wound site morbidity and loss of function from that nerve), ANAs, and NGTs. While these graft strategies provide a substrate for axon extension and support cell migration into the defect between the host nerve stumps, these current repair strategies are largely ineffective for major nerve trauma (loss of ≥5 cm of nerve and/or proximal nerve injury). Despite decades of work, the autograft remains the gold standard for nerve repair, and NGTs are only indicated for small-gap nerve repair (*5*). In contrast to existing strategies, TENGs use living neurons with preformed axon tracts to bridge segmental defects, while TENG neurons also project new axons to potentially babysit the otherwise denervated distal nerve. Therefore, unlike other approaches lacking transplantable axons, TENGs may overcome the major challenges that currently limit functional recovery in the clinical setting.

To assess whether TENGs can babysit axotomized host Schwann cells, we initially used a rodent model of chronic axotomy following transection that prevented host axonal ingrowth into the distal stump. As expected, chronic denervation resulted in a marked reduction in Schwann cell alignment over several weeks and an almost complete loss of Schwann cell presence by 16 weeks after injury. To combat the degeneration of distal Schwann cells, one of the major challenges for successful nerve regeneration, TENGs were attached to the transected distal nerve to determine whether TENG axon outgrowth and the associated neurotrophic support could maintain host Schwann cells over 16 weeks. Out to 16 weeks after transplantation, TENG neurons survived and extended axons deep into the distal nerve structure that directly interacted with host Schwann cells. This axon penetration from transplanted TENGs corresponded with maintenance of distal host Schwann cells over extended time periods compared to NGT-only controls in an otherwise denervated peripheral nerve. Notably, TENG axons were found at considerable distances from the transplanted cell body located in the graft region following chronic host axotomy (up to 3 cm, the longest distance that we could examine in rats). However, TENG axons were relatively sparse compared to the total fascicular area, showing that relatively few axons extending from transplanted neurons are required to maintain proregenerative Schwann cell columns over time (see Fig. 2F). This suggests that there may be additional, currently undefined, signaling mechanisms between Schwann cells directly interacting with TENG axons and Schwann cells not contacting TENG axons, for instance, the secretion of neurotrophic factors from Schwann cells directly stimulated by transplant axons, that are able to maintain other host Schwann cells in a proregenerative, aligned state. Notably, the columnar alignment of Schwann cells is important for accurate guidance of the regenerating axons to appropriate targets; without this guidance, axons may occasionally grow along the epineuria directly onto the denervated muscle surface, resulting in poor reinnervation (*30*). Although our rodent data provide justification for translation to a large animal study, future studies may include testing the effects of TENG axons in otherwise denervated

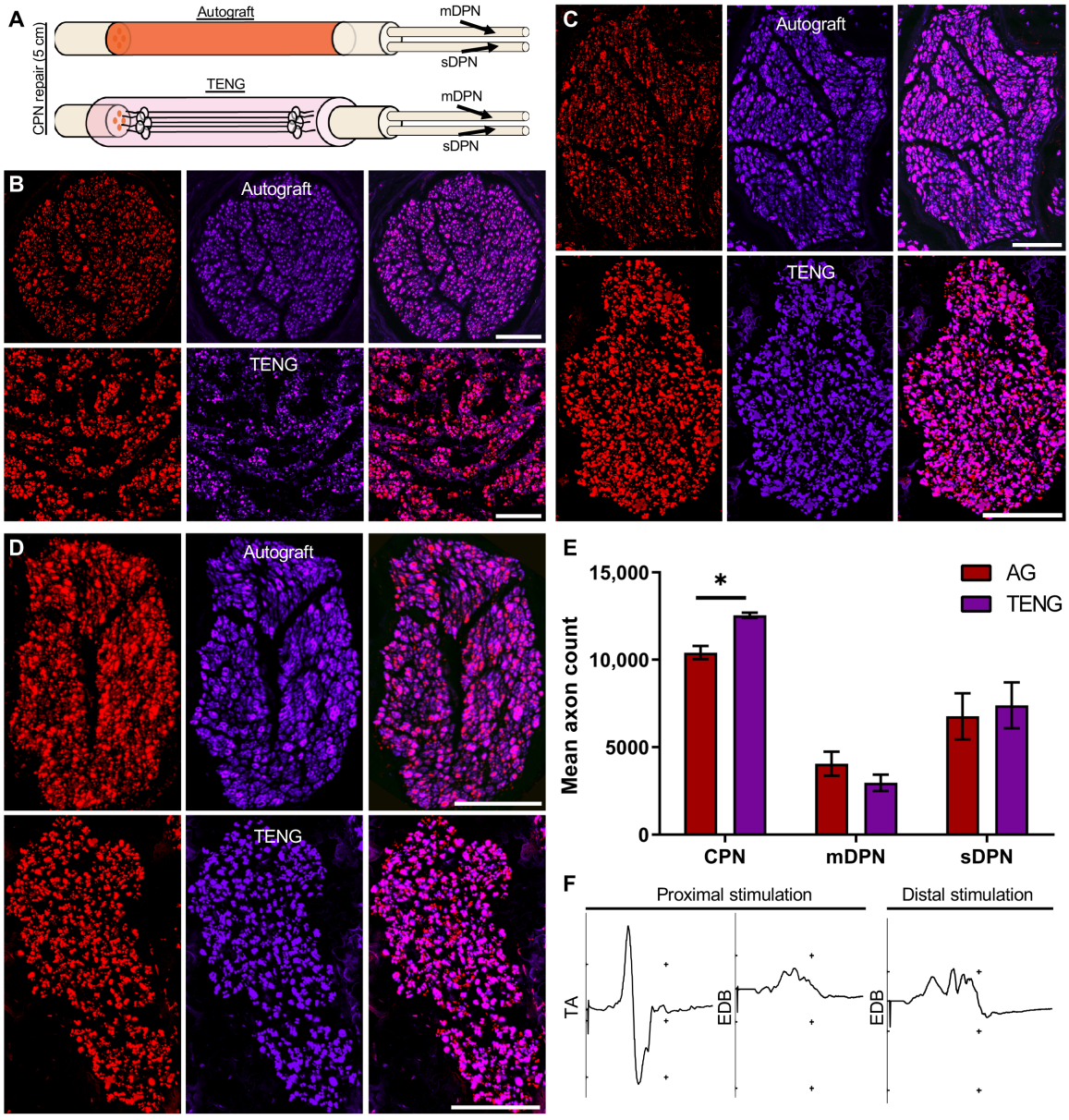

Fig. 8. Axon regeneration and functional reinnervation at 12 months following repair of 5-cm CPN segmental defects in swine. (**A**) In this study, a 5-cm CPN segmental defect was repaired using a TENG (with or without distal babysitter grafts) or autograft. (**B** to **D**) Immunohistochemistry of a single representative fascicle of the (B) CPN segment distal to the repair zone, (C) mDPN, and (D) sDPN revealed successful axonal regeneration across the challenging defect and ongoing axon maturation. (**E**) Mean axon counts following TENG versus autograft repair for the repaired nerve (CPN) and two distal branches (mDPN and sDPN). (**F**) CMAPs were recorded from both muscles innervated by branches of the CPN: the tibialis anterior (TA; innervated ~8 cm distal to the primary repair zone) and the EDB (innervated ~27 cm distal to the primary repair zone). Nerve stimulation proximal and distal to the repair site elicited robust muscle movement, and positive hoof eversion was observed, corroborating the CMAP recordings. *P* values are represented as $*P < 0.05$. Scale bars, 100 μm. Divisions, 500 μV/25 ms. $n = 3$ for both groups at 12 months after repair.

nerve sheaths over time and whether TENG implants can rescue the denervated nerve following transplantation at the time of a delayed primary repair procedure. With these caveats, our current findings suggest that TENGs were capable of preserving the proregenerative environment within the distal nerve necessary to enable host axons to reach long-distance targets.

The next phase of these studies evaluated whether the primary mechanism of action of TENGs (i.e., AFAR) previously observed in a rodent model was also relevant in a porcine model. On the basis of our previous rodent studies, we expected that TENGs would serve as an axon-based living scaffold to facilitate nerve regeneration via two complementary mechanisms: (i) AFAR, whereby host axons grow directly along TENG axons even in the absence of Schwann cells, and (ii) enhancement of Schwann cell infiltration and alignment, which, in turn, accelerates host axon regeneration along these Schwann cells. To evaluate acute regeneration, axon regeneration and Schwann cell infiltration were measured at 2 weeks following 1-cm repair of the sDPN and mDPN. Notably, the rate of axon

regeneration across TENGs was statistically equivalent to that of autografts and 4.2- and 1.6-fold faster than that of NGTs following repair of the sDPN and mDPN, respectively. Thus, the rates of axon outgrowth for autografts and TENGs were vastly superior to that of NGTs in both motor and sensory nerves. While the focus of these initial studies was on the effects of TENG axons on the acute rates of host axonal regeneration, future studies should also evaluate the density of regenerating axons as a function of distance within the graft to provide additional context.

The current TENGs (built using sensory neurons) achieved greater regeneration across the graft zone when used to repair the sDPN (regenerative front: 1.2 mm/day; leading regenerators: 1.5 mm/day) as compared to the mDPN (regenerative front: 0.4 mm/day; leading regenerators: 1.0 mm/day), suggesting a modality preference for AFAR that warrants additional study. We also found accelerated Schwann cell infiltration within TENGs compared to NGTs, although levels of TENG-mediated infiltration were similar following repair of sDPN and mDPN (1.2- and 1.3-fold increase, respectively). These findings suggest that TENGs accelerate regeneration across the graft and Schwann cell infiltration from the host nerve stumps. The precise mechanisms that enable TENGs composed of sensory axons to improve regeneration of both sensory and motor nerves remain unclear, although the trend toward accelerated regeneration of sensory axons may be due to the inherently faster growth capacity of sensory axons compared to motor axons and that sensory axons may preferentially extend along other sensory axons (thus better leveraging AFAR in sensory TENGs). Hence, further investigation is warranted to test whether modality-specific TENGs (i.e., TENGs composed of stretch-grown sensory neurons, motor neurons, or sensory and motor neurons) improve regeneration and recovery when used to repair modality-matched nerves. Similarly, note that in the current study, the sDPN was repaired using a reverse autograft, matching a standard practice for preclinical experimentation, whereas the mDPN was repaired using the sural nerve autograft, matching the standard clinical procedure. While it was not a goal of the current study to directly compare regeneration between motor and sensory nerves, future studies could apply this porcine model to elucidate whether nerve graft modality (relative to repaired nerve, e.g., motor autograft for motor nerve reconstruction and sensory autograft for sensory nerve reconstruction) influences factors such as host axon regeneration, axon–Schwann cell interactions, and/or axon maturation.

We next evaluated whether TENGs could facilitate regeneration and electrophysiological recovery across a long-gap (5-cm) injury to the mDPN, a predominantly motor nerve ~20 cm from the target muscle. Allogeneic TENG neurons and axons were found many months after repair despite the lack of immunosuppression. As early as 3 months following TENG repair, CNAPs were recorded across the 5-cm deficit, which was corroborated histologically via axon regeneration and restored nerve architecture within and distal to the graft region. Furthermore, nerve stimulation elicited an evoked muscle response and observable hoof twitch at chronic time points (as early as 7 months). Dense regenerating myelinated and unmyelinated axons were visualized within the distal nerve and entering the target muscles, supporting the findings of electrophysiological recovery. Collectively, these data demonstrate that TENGs facilitate nerve regeneration and electrophysiological recovery following repair of 5-cm lesions in swine at similar levels to those attained by conventional repairs using the sural nerve autograft. However, electrophysiological experiments are particularly challenging following long-gap nerve repair, often requiring meticulous electrode placement and precise stimulation to minimize the potential for nonspecific activation (*31*). Future studies using this paradigm could also include agents to silence the regenerated nerve (e.g., lidocaine) following standard electrophysiological assessments to further ensure the specificity of the evoked response.

For clinical deployment, we envision a dual-transplantation strategy with secondary babysitting TENG(s) distal to a primary repair to preserve the proregenerative Schwann cells ahead of regenerating axons. We predicted that axonal processes extending from babysitting TENGs would be beneficial by maintaining the proregenerative environment of the distal segment as the host axons regenerated across the long gap. To demonstrate a potential TENG dual-transplantation strategy, we evaluated regeneration across a challenging, clinically relevant long-gap (5-cm) nerve injury in the CPN, a large-diameter mixed motor-sensory nerve. Compared to the DPN model, the CPN injury requires greater regenerative distances because of its more proximal location further from the end target (~20 cm versus ~27 cm). In this model, the segmental defect in the CPN was repaired using a TENG or saphenous nerve autograft. At 12 months after repair, evoked muscle electrophysiological responses were obtained, indicating that sufficient regeneration had occurred for reinnervation. These findings were corroborated with histological evidence that showed that regenerating axons crossed the graft region and entered into the distal branches, ~8 cm distal to the initial 5-cm defect. Greater axon counts (but with equivalent maturation) were observed in the distal CPN following TENG repair compared to autografts; however, there were no significant differences in axon density in the distal branches. While these findings are encouraging, further studies are required to ascertain the performance of TENGs versus autografts in even more challenging scenarios, such as even longer segmental defects or common delayed surgical repair cases. Moreover, a limitation of the current study is that complete functional recovery based on behavioral sensorimotor outcome metrics (e.g., gait analysis and/or return of pain/temperature/pressure sensation) was not assessed, but these critical outcome measures should be featured in future safety and efficacy testing of TENG-mediated nerve regeneration.

In the cohort that received two 0.5-cm babysitting TENGs in continuity with the mDPN, approximately 3 and 8 cm distal to the distal end of the repair zone, robust TENG axon outgrowth was widespread throughout the mDPN. As expected, there were subtle differences in the ongoing axon maturation and myelination process across treatment groups. While no significant differences were found for *g*-ratio distribution profiles of axons in the mDPN branch distal to the primary 5-cm CPN repair, the autograft and TENG + BS *g*-ratio profiles were more similar to the naïve contralateral mDPN *g*-ratio profile. This may suggest that the TENG + BS repair paradigm potentially hastens axon maturation, although further study is warranted. Histological analyses also revealed that the density of TENG axons was proportional to the density of the regenerated axons, suggesting a "dose effect" to provide distal nerve preservation. These findings suggest that TENG axons may support a proregenerative environment and preserve the capacity for host axonal regeneration, although future work is necessary to investigate whether these subtle differences affect the rate or ultimate extent of functional recovery. Overall, these findings support further exploration of this dual–tissue engineering transplantation strategy that may allow host

axons to reinnervate long-distance targets and potentially facilitate functional recovery following challenging PNI repair scenarios.

Few studies have demonstrated a successful long-gap nerve repair in a large animal model. Recent advancements have led to the development of next-generation conduits, such as biodegradable polymer nerve guides composed of poly(caprolactone) (PCL) embedded with glial-derived neurotrophic factor (GDNF) that is encapsulated within double-walled, poly(lactic-co-glycolic acid)/poly(lactide) microspheres (*32*). These nerve guides have shown promising regeneration and functional recovery in a 1.5-cm rodent nerve injury model and a 5-cm median nerve nonhuman primate model (*32*, *33*). Similar to our findings with TENGs, nerve repair with PCL conduits loaded with microspheres containing GDNF did not result in greater electrophysiological recovery than the autograft. Although this work is promising, autografts will likely remain the gold standard for clinically challenging cases requiring a nerve bridge until an alternative approach demonstrates superior efficacy. However, note that although regeneration across the defect is necessary for successful reinnervation, meaningful recovery requires the axons extending from the regenerating proximal neurons to be able to successfully reinnervate the distal muscle. Therefore, future work should aim to further optimize bridging strategies (e.g., TENGs) coupled with babysitting strategies to ensure pathway protection and end target vitality.

While the current study focused on babysitting resident Schwann cells to ensure that regenerating axons have targeted axon guidance for appropriate reinnervation, there are currently no clinically available strategies that aim to maintain muscle functionality. With extended denervation times, the distal nerve segment not only becomes less supportive of regenerating axons, but the denervated end targets become nonviable for reinnervation. Here, denervation atrophy of target muscles is a major problem as skeletal muscles gradually degrade and lose receptivity to regenerating axons. The clinical "rule of thumb" is that the potential for reinnervation diminishes by ~1% per week, rendering targets unable to accept regenerating axons over time, even if axons reach muscle targets. In this case, additional neuron subtypes may need to be transplanted (e.g., primary or stem cell–derived spinal motor neurons with or without sensory neurons) to better match the modality of the nerve and allow end target innervation (*34*). These neuronal constructs may be delivered to the end of a transected nerve (e.g., within an NGT) or directly injected into individual nerve fascicles (*35*). Moreover, although the current studies have established that babysitting TENGs can maintain the aligned structure of resident Schwann cells following acute transplantation, clinical situations often require a delay between primary injury and repair, ranging from weeks to months. Therefore, although transplanted TENG neurons survive transplantation and thrive in vivo, future studies are necessary to investigate whether TENGs preserve the Schwann cell architecture not only following acute transplantation but also when delivered weeks or months after axotomy.

On the basis of our findings, TENGs have a novel mechanism of action compared to empty NGTs, ANAs, autografts, and other experimental tissue engineering strategies that aim to create permissive scaffolds containing hydrogels, aligned fibers, extracellular matrix, trophic factors, and/or glial or stem cells (*36*). AFAR is a newfound form of axon regeneration, unique to TENGs, which complements traditional Schwann cell–mediated axon regeneration. In addition, TENG axons were found as early as 2 weeks after repair extending far into the distal nerve stumps, indicating the potential to maintain a proregenerative Schwann cell phenotype, an essential process for long-distance targeted regeneration, ahead of the regenerative host axons. These mechanisms of action, whereby TENGs facilitate both accelerated axon regeneration across the graft via AFAR and sending axons into the distal nerve to prolong its proregenerative ability, are the key differentiators from other PNI repair strategies, including the autograft. Moreover, our findings that AFAR is a relevant mechanism of action following TENG repair in pigs may suggest applicability of this mechanism following nerve injury in humans. These considerations are important since there is a relatively short time frame after nerve transection, which results in degeneration of the distal axons that have been physically disconnected from their proximal cell bodies, that presents a chance for functional recovery (*30*, *37*–*39*). TENGs appear to promote greater Schwann cell infiltration (into the graft zone) and/or maintenance (distal to the graft zone) with an aligned columnar formation, which likely results in elevated synthesis and secretion of proregenerative neurotrophic factors, such as nerve growth factor, brain-derived neurotrophic factor, and neurotrophin-3 (NT-3) (*30*, *40*–*43*), while also preventing the disintegration of the Schwann cell basal lamina (*44*). Unlike other strategies, TENGs appear to mitigate host Schwann cell senescence for long gaps, a concern that has been expressed for alternative PNI repair strategies (*45*). As an engineered "living scaffold," the neurotrophic and structural support provided by TENGs likely encouraged axonal growth not only directly along TENG axons but also along host Schwann cells that had fully infiltrated the graft region and subsequently into the bands of Büngner, toward reinnervation of appropriate distal targets.

ANAs, such as the Avance product, are a commercially available alternative to the autograft that are composed of decellularized human cadaveric nerve and are often used in distal sensory nerve reconstruction (*46*, *47*). While ANAs are a popular alternative, unlike autografts and TENGs, ANAs are nonliving scaffolds that require Schwann cell infiltration before axonal regrowth can ensue, and it appears that Schwann cells must fully cross the graft to enable successful axonal extension across the repair zone (*45*, *48*). Moreover, ANAs have been reported to have poor regeneration in cases of long-gap nerve repair, likely because Schwann cells infiltrating the graft undergo senescence before axons completely regenerate across the graft and/or undergo maturation (*45*, *48*). The lack of endogenous Schwann cell support (as provided by autografts) or lack of exogenous axons for AFAR (as provided by TENGs) may ultimately result in diminished regeneration across ANAs, especially in cases of long-gap nerve reconstruction. Nonetheless, future studies should leverage this clinically relevant large animal model to directly compare the efficacy of commercially available nonliving scaffolds (e.g., Avance grafts) versus living scaffolds (e.g., clinical-grade TENGs), each benchmarked to the clinical gold standard of the sensory nerve autograft for surgical repair of a critical motor nerve.

Successful translation requires selecting an appropriate starting biomass for scale-up and eventual safety and efficacy testing in a clinical trial. In this study, we demonstrate that allogeneic pig TENGs survive in vivo without the use of immunosuppressive agents; however, it remains unclear why TENG neurons/axons appear to be spared from a significant immune response. One reason may be that the nervous system has some inherent immune privilege. Another explanation may be that the embryonic cells are well tolerated and/or induce a reduced immunological response. While the exact

mechanism that facilitates allogeneic neuron survival remains unknown, this work provides an important step toward future translation, which will include initiating a clinical-grade manufacturing process using an appropriate cell source to facilitate investigational new drug (IND)-enabling nonclinical testing and then clinical trials. Here, cell source selection will be critical and will strongly influence whether an immunosuppressive agent must be used in conjunction with TENG-mediated nerve repair procedures done clinically. For instance, nongenetically modified allogeneic neurons and/or xenogenic neurons may require immunosuppression, which may also affect regenerative processes and could increase the risk of postoperative infection. Although human stem cells are a potential option for TENG fabrication, long derivation protocols combined with prolonged stretch-growth periods might lead to delays in surgical repair. Therefore, we have begun proof-of-concept and efficacy testing using TENGs composed of genetically engineered porcine neurons designed to be hypoimmunogenic in humans and mitigate acute rejection (*49*–*52*). Despite these advancements in genetic engineering, as a xenogenic cell source, a mild immunosuppressant, such as FK506, might be required. Notably, FK506 administration has been shown to facilitate nerve regeneration, which may further improve regenerative outcomes when combined with TENG repair (*53*–*56*). Moreover, immune suppression can likely be gradually tapered off to allow for the removal of the porcine neurons as TENGs are only needed temporarily (e.g., over the course of several months) to facilitate axon regeneration. If shown to be safe and efficacious, TENGs will offer surgeons an alternative reconstruction strategy without the inherent drawbacks associated with an autograft or nerve transfers (e.g., limited availability and comorbidity), thus providing a transformative therapy to address complex and severe PNI.

This work demonstrates TENGs as the first axon-based living scaffold to facilitate peripheral nerve regeneration across long lesions and enable long-distance reinnervation. TENGs mimic developmental mechanisms to facilitate axon regeneration and Schwann cell infiltration across long segmental defects, attaining levels of nerve regeneration and electrophysiological function at least equal to that of the "gold-standard" sensory nerve autograft in challenging porcine models of PNI. TENGs were shown to be superior to conventional commercially available bridging strategies such as NGTs by promoting robust and accelerated axon regeneration across segmental defects, resulting in an accelerated recovery response. While TENGs matched or exceeded the performance of the autograft, TENGs uniquely offer the ability to project local axons to maintain the pro-regenerative distal pathway, which may be necessary for axon regeneration and target innervation in even more challenging nerve repair scenarios. In addition, TENGs can be an off-the-shelf product and thus not necessitate the harvest of an otherwise uninjured nerve, thereby avoiding the deliberate infliction of a deficit on the patient. On the basis of these promising large animal studies, the next steps in the translation of TENGs involve the transition to a clinical-grade biomanufacturing process to support IND-enabling preclinical safety studies. If successful, TENGs could improve outcomes compared to conventional approaches and potentially be applied for nerve damage that is so extensive that repair is not currently attempted.

MATERIALS AND METHODS

All procedures were approved by the Institutional Animal Care and Use Committees at the University of Pennsylvania and the Corporal Michael J. Crescenz Veterans Affairs Medical Center and adhered to the guidelines set forth in the National Institutes of Health Public Health Service Policy on Humane Care and Use of Laboratory Animals (2015).

Biofabrication of TENGs

Rodent TENGs for allogeneic transplant were generated using DRG neurons harvested from embryonic day 16 (E16) fetuses from timed-pregnant Sprague-Dawley females (Charles River Laboratories). Whole-DRG explants were cultured and stretch-grown to 1 cm as previously described (*25*, *26*, *57*). Immunohistochemistry was performed on a subset of cultures as previously described (*25*, *26*, *57*).

Allogeneic pig TENGs were generated using DRG neurons isolated from E40 fetuses from timed-pregnant sows expressing GFP (strain NSRRC:0016, National Swine Resource and Research Center). Whole-DRG explants were cultured in Neurobasal medium supplemented with 2% B-27, 500 μM L-glutamine, 1% fetal bovine serum (Atlanta Biologicals), glucose (2.5 mg/ml; Sigma-Aldrich), 2.5S nerve growth factor (10 ng/ml; BD Biosciences), 10 μM 5FdU (Sigma-Aldrich), 20 μM uridine (Sigma-Aldrich), and 0.1% penicillin-streptomycin. Pig axons were stretch-grown to fabricate babysitting TENGs (0.5 cm) or bridging TENGs (1 or 5 cm).

DRGs were plated within custom-built mechanobioreactors designed for the stretch growth of integrated axonal tracts as previously described (*25*, *26*, *57*). For rodent neuronal cultures, two Aclar membranes were treated with poly-D-lysine (20 μg/ml; BD Biosciences) and laminin (20 μg/ml; BD Biosciences). For pig cultures, membranes were treated with poly-D-lysine (40 μg/ml) and laminin (40 μg/ml). The "towing membrane" was attached to the stepper motor, and the "base membrane" remained fixed during stretch. Two populations of DRGs were plated in a row on opposite sides of the membrane interface approximately 1 mm apart (*25*). For 0.5- or 1-cm TENGs, a 1-cm-wide towing membrane was used, and 10 DRGs were plated on the towing membrane and 10 DRGs on the base membrane. For 5-cm TENGs, a 2-cm-wide towing membrane was used, and 20 DRGs were plated on the towing membrane and 20 DRGs on the base membrane.

At 5 days in vitro (DIV), the microstepper was engaged to separate the DRG populations until the desired lengths. For 0.5-cm TENGs, the stretch rate was 1 mm/day for 5 days. For 1-cm TENGs, the stretch rate was 1 mm/day for 2 days and then increased to 2 mm/day for 4 days. For 5-cm TENGs, the stretch paradigm was as follows: 1 mm/day for 1 day, 2 mm/day for 2 days, and 3 mm/day for 15 days. A half medium change was completed once every week. Once the terminal length was reached, the DRG and axon tracts were carefully examined under phase-contrast and fluorescent microscopy.

Stretch-grown cultures deemed transplantable by a semiquantitative neuronal/axonal health score were encapsulated in an extracellular matrix as previously described (*25*, *26*, *57*). After gelation at 37°C, embedded cultures were removed from the membranes, rolled, and placed within a nerve guidance conduit. Rat TENGs were encapsulated in rat-tail collagen type I (3.0 mg/ml; BD Biosciences) supplemented with 2.5S nerve growth factor (0.05 μg/ml; BD Biosciences) and encased in a 1-cm Stryker Neuroflex NGT. Pig TENGs were encapsulated in pig collagen type I (3.0 mg/ml; Elastin Products Company) in minimum essential media (Invitrogen) supplemented with 2.5S nerve growth factor (0.05 μg/ml; BD Biosciences). Pig TENGs up to 1 cm long were encased within an NGT, and 5-cm-long

pig TENGs were encased within a Stryker NeuroMend nerve wrap or Baxter/Synovis NeuroTube.

Rodent peripheral nerve surgery and transplantation in a chronic axotomy model

Sprague-Dawley rats (weight, 300 to 330 g; male; $N = 20$ in total) were used in the chronic axotomy studies. Anesthesia was maintained under isoflurane for the entire duration of the surgery. Bupivacaine (2 mg/kg) was administered along the incision line. Meloxicam (2 mg/kg) was administered preoperatively and for 2 days postoperatively. The sciatic nerve was exposed using a split-muscle approach and was transected 1 cm proximal to the trifurcation. The distal stump was secured to either a 1-cm NGT or TENG using 8-0 Prolene sutures.

The chronic axotomy model aims to mimic the features found after nerve injury resulting in prolonged periods of denervation due to the absence of axonal contact in the distal nerve. In this study, we evaluated the efficacy of TENGs to provide early reinnervation in an otherwise denervated distal nerve. To create a model of chronic axotomy, the proximal stump was capped using nonresorbable latex to prevent inadvertent regeneration of the proximal stump into the transection site. GFP^+ TENGs or empty NGTs were sutured to the distal nerve stump. Muscle and skin layers were closed using absorbable chromic gut 4-0 sutures. Terminal survival times ranged from 2 to 16 weeks following NGT implants ($n = 16$ total) or 16 weeks following TENG implants ($n = 4$).

Porcine peripheral nerve surgical approach for 1- or 5-cm segmental nerve repair model

Yorkshire pigs (3 months old, 25 to 35 kg, female; Animal Biotech Industries; $N = 25$ pigs in total) were used in the short-gap regeneration experiment (1-cm repair over 2 weeks), and Yucatan minipigs (5 to 6 months old, 25 to 35 kg, female; Sinclair Bio Resources; $N = 38$ pigs in total) were used in the long-gap regeneration experiments (5-cm repair). Animals were fasted overnight and were initially anesthetized intramuscularly with a ketamine (20 to 25 mg/kg) and midazolam (0.4 to 0.6 mg/kg) cocktail. All animals were intubated and maintained under general anesthesia (2.0 to 2.5% isoflurane at 2 liters/min). All surgical procedures were performed under general anesthesia and followed aseptic technique. Following repair, the deep layers and skin were closed, and a sterile bandage was placed over the incision site with triple antibiotic ointment. Local anesthetic and preoperative and postoperative analgesia were administered as previously described (*31*). Vital signs were continuously monitored in all animals during the procedure.

Segmental short-gap (1-cm) defect of DPN repaired with TENG, NGT, or nerve autograft

The sDPN and mDPN were exposed as previously described (fig. S1) (*31*). For TENG or NGT repairs, the two nerve stumps were inserted into the ends of the TENG or NGT and sutured to the epineurium using four 8-0 Prolene sutures. Fibrin sealant (Tisseel, Baxter Healthcare, Deerfield, IL) was applied at the margins and longitudinally. For the sDPN autograft repair, a 1-cm segment was cut and positioned 180° relative to the normal proximal-distal direction, and a tensionless reverse autograft repair was completed using two 8-0 Prolene simple interrupted epineural sutures secured to each end (*58*). For the mDPN autograft repair, the donor sural nerve was harvested and sutured in place for a tensionless repair as described previously (*31*). Experimental groups were as follows: segmental defect in sDPN [autograft repair ($n = 4$), NGT repair ($n = 4$), and TENG repair ($n = 5$)] and segmental defect in mDPN [autograft repair ($n = 4$), NGT repair ($n = 4$), and TENG repair ($n = 4$)]. Animals survived to an acute 2-week time point.

Segmental long-gap (5-cm) defect of DPN (~20 cm from target muscle) repaired with TENG or sural nerve autograft

The mDPN was exposed as described previously (*31*), and a 4.8-cm segment was excised. For TENG repairs, a 5-cm TENG was transplanted in the defect with a 1-mm overlap as described above. For mDPN autograft repairs, a donor sural nerve was reversed, trimmed to 5 cm, and sutured in place for a tensionless repair as described previously (*31*). Experimental groups for the 5-cm mDPN segmental defects were as follows: autograft repair ($n = 6$) and TENG repair ($n = 10$). Animals were euthanized at subacute (1 month), intermediate (3 to 6 months), or chronic (7 to 11 months) time points after repair.

Segmental long-gap (5-cm) defect of CPN (~27 cm from target muscle) repaired with TENG or saphenous nerve autograft

The CPN and the distal branches of the DPN were exposed as previously described, and the CPN was transected 5 cm proximal to the bifurcation of the distal branches, and a 4.0-cm nerve segment was removed (*31*). The primary CPN repair was completed using either a 5.0-cm sensory nerve autograft or a 5.0-cm TENG encased within a nerve wrap. For CPN autograft repairs, a tensionless reverse autograft was completed using a donor saphenous nerve trimmed to 5 cm (which better matched the diameter of the CPN than the sural nerve) (*31*). For TENG repairs, the defect was repaired as described above. A subset of animals also received babysitting TENGs implanted at secondary repair sites in the mDPN. Here, the mDPN was sharply cut at two points, and 0.5-cm TENGs were implanted across each, with suturing as described above. The proximal babysitting TENG was placed 0.5 cm distal to the bifurcation. The distal babysitting TENG was implanted 0.5 cm proximal to the point that the DPN courses under the flexor retinaculum. The distance between the centers of the two constructs was approximately 5.5 to 6.0 cm. Experimental groups for the 5-cm CPN segmental defect were as follows: CPN repair with autograft ($n = 7$), CPN repair with TENG ($n = 11$), and CPN repair with TENG plus two babysitting TENGs in mDPN ($n = 4$). Animals were euthanized at intermediate (3 to 6 months) or chronic (12 months) time points after repair.

Muscle and nerve electrophysiological evaluation

Following nerve repair, evoked muscle and nerve responses were measured similarly to previously established methodology (*31*). CMAPs were recorded using a subdermal electrode placed in the EDB following nerve stimulation (biphasic; amplitude: 0 to 10 mA; duration: 0.2 ms; 100× gain; band-pass filter: 10 to 2000 Hz) with a handheld bipolar hook electrode (*31*). CMAPs were recorded following stimulation 5 mm proximal and distal to the repair site. The stimulus intensity was increased to obtain a supramaximal CMAP. CMAP baseline-to-peak amplitude was measured from the waveform averaged across a train of five pulses.

CNAPs were recorded with a bipolar electrode (Medtronic, #8227410) following stimulation across the repair zone (biphasic; amplitude: 0 to 1 mA; duration: 0.2 ms; 1000× gain; band-pass filter: 10

to 10,000 Hz) with a handheld bipolar hook electrode (*31*). CNAP peak-to-peak amplitude was measured from the waveform averaged across a train of five pulses.

Euthanasia, tissue processing, and histology

At the conclusion of all studies, animals were deeply anesthetized and subsequently euthanized by Euthasol (rodents) or transcardial perfusion with formalin and phosphate-buffered saline (PBS; pigs). For the rodent experiments, subjects were anesthetized, and the graft region and the distal sciatic nerve were harvested at terminal time points. Nerves were postfixed in formalin at 4°C overnight. Formalin-fixed nerves were cryoprotected for 48 hours in 30% sucrose in PBS, frozen in optimal cutting temperature media, and cryosectioned either longitudinally (20 μm) along the graft region or axially (10 μm) starting 0.5 cm distal to the graft zone. Rodent histological analyses were performed up to 16 weeks after transection to determine distal nerve Schwann cell presence, cytoarchitecture, graft survival, and graft axon integration with distal nerve.

At the terminal time points of porcine studies, ipsilateral and contralateral hindlimbs were postfixed in formalin at 4°C overnight, and then nerves were harvested and postfixed in formalin at 4°C overnight. For the short-gap study (1-cm graft; 2 weeks after repair) and the early regenerative phase cohort in the long-gap study (5-cm graft; 1 and 3 months after repair), nerves were cryoprotected and frozen. Sections were taken longitudinally (20 μm) across the graft or axially (10 μm) at 1-cm intervals along the length of the nerve beginning at 0.5 cm distal to the graft zone. Frozen sections were washed three times in PBS, blocked, and permeabilized in 4% normal horse serum with 0.3% Triton X-100 for 1 hour. All subsequent steps were performed using blocking solution for antibody dilutions. Axons were labeled with anti-NF200 (1:200; Sigma-Aldrich, N0142) and/or anti-SMI31/32 (1:1500; Millipore, NE1022/NE1023). Schwann cells and myelin were labeled with anti-S100 (1:250; Dako, Z0311) and anti–myelin basic protein (MBP; 1:1500; Encor, CPCA-MBP), respectively. Primary antibodies were applied overnight at 4°C followed by the appropriate fluorophore-conjugated secondary antibody (1:1000; Alexa Fluor, Invitrogen) for 2 hours at room temperature. For animals enrolled in the long-gap cohort studying the chronic regenerative phase (5-cm defects, 6 to 12 months after repair), formalin-fixed nerves were paraffin-embedded, and axial sections (8 μm) were taken at 1-cm intervals along the length of the nerve beginning at 0.5 cm distal to the graft zone. Deparaffinized sections were rehydrated in descending ethanol gradient, and high-heat and pressure antigen retrieval was performed in tris/EDTA buffer. Sections were blocked with 4% normal horse serum in OptiMax (BioGenex, HK583-5K). All subsequent steps were performed using blocking solution for antibody dilutions. Sections were incubated with primary antibodies for axons, Schwann cells, and myelination as described above.

Microscopy, quantification, and statistical analyses

Neuronal constructs in vitro were imaged using phase-contrast or epifluorescence microscopy on a Nikon Eclipse Ti-S with digital image acquisition using a QIClick camera interfaced with Nikon Elements Basic Research software (4.10.01). For immunolabeled neuronal constructs, fluorescent imaging was completed using a Nikon Eclipse Ti-S or Nikon A1R confocal microscope.

All histological analyses were performed by trained scientists blinded to group identity. Longitudinal and axial tissue sections were imaged with a Nikon A1R confocal microscope (1024 × 1024 pixels) with a 10× air objective or 60× oil objective interfaced with Nikon NIS-Elements AR 3.1.0 (Nikon Instruments, Tokyo, Japan). Multiple confocal *z*-stacks were digitally captured and analyzed, with all reconstructions tiled across the full section and full *z*-stack thickness.

Schwann cell morphology in the distal nerve following chronic axotomy in rats was assessed from multiple high-resolution confocal reconstructions per animal. A semiquantitative scoring system was applied by two researchers blinded to the experimental group: 5, robust, aligned Schwann cells; 4, aligned Schwann cells; 3, reduced Schwann cells, semi-aligned; 2, scattered Schwann cells, little alignment; and 1, few/no Schwann cells, loss of alignment. This analysis was performed on the full cohort at the following time points: 2, 4, 6 to 8, 9, and 16 weeks after implant (NGT only, $n = 3$ to 4 rats per time point) or 16 weeks after implant (TENG, $n = 4$ rats).

In porcine experiments at the acute and subacute time points, axon regeneration and Schwann cell infiltration were measured from longitudinal sections including the 1-cm graft at 2 weeks after repair and the 5-cm graft at 1 month after repair using previously established methodology (*26*). Briefly, the length of the host axons (SMI31/32) was measured from the proximal end of the repair zone with TENG axons noted to be GFP^+ (*26*). Host axons were grouped as the regenerative front, main bolus of regenerating host axons, or the leading regenerators, the longest-projecting host axons. Schwann cell infiltration was measured on the basis of the $S100^+$ coverage from both the proximal and distal ends of the graft. This quantitative analysis was performed on the full cohort of 1-cm lesion repairs at 2 weeks after repair: sDPN segmental defect repaired with autograft ($n = 4$ pigs), NGT ($n = 4$), and TENG ($n = 5$); mDPN segmental defect repaired with autograft ($n = 4$), NGT ($n = 4$), and TENG ($n = 4$). At 1 month following repair of 5-cm lesions in the mDPN, this quantitative analysis was performed in animals repaired with autograft ($n = 2$ pigs) or TENG ($n = 3$).

In porcine experiments at intermediate time points following repair of 5-cm lesions in the mDPN or CPN, axon regeneration and Schwann cell presence/morphology were qualitatively assessed in longitudinal sections in the graft region and axial sections distal to the graft region. At chronic time points, axon regeneration and myelination were quantitatively assessed using axial sections distal to the graft region. Here, the total number of axons was determined by quantifying the number of neurofilament-positive axons. TENG axons were identified as GFP^+ axons. The percentage of myelinated (MBP^+) axons was also quantified. This quantitative analysis was performed in the chronic cohorts following 5-cm segmental defects in the mDPN repaired with autograft ($n = 3$ pigs) or TENG ($n = 5$) and in the CPN repaired with autograft ($n = 3$) or TENGs ($n = 3$; with or without distal grafts). Axon regeneration and Schwann cell presence/morphology were also qualitatively assessed at chronic time points, from longitudinal sections immediately distal to the babysitting grafts (in animals receiving these grafts).

All quantitative data (e.g., mean Schwann cell morphology, axon regeneration, Schwann cell infiltration, and axon myelination) were compared using either Student's *t* test or one-way analysis of variance (ANOVA). When differences existed between groups following ANOVA, Tukey's post hoc pairwise comparisons were performed. Axon fiber diameter and *g*-ratio for myelinated axons (ratio of the inner axonal diameter to the total outer diameter) were also calculated by sampling three 100-μm^2 areas. At least 100 measurements were obtained per animal. Data were binned in 0.5-μm increments

from 0.5 to 7 μm (axon diameter) and 0.05 increments from 0.3 to 0.9 (*g*-ratio). The cumulative frequency distribution was plotted with the nonlinear Gaussian line of best fit. Myelinated axon diameter and *g*-ratio histograms were compared using the two-sample Kolmogorov-Smirnov test to evaluate the agreement between distribution profiles. For all statistical tests, $P < 0.05$ was required for significance (GraphPad Prism, La Jolla, CA, USA). Mean values are presented as means ± SEM unless otherwise noted.

SUPPLEMENTARY MATERIALS

Supplementary material for this article is available at https://science.org/doi/10.1126/sciadv.abm3291

View/request a protocol for this paper from *Bio-protocol*.

REFERENCES AND NOTES

1. D. Grinsell, C. P. Keating, Peripheral nerve reconstruction after injury: A review of clinical and experimental therapies. *Biomed. Res. Int.* **2014**, 698256 (2014).
2. C. A. Taylor, D. Braza, J. B. Rice, T. Dillingham, The incidence of peripheral nerve injury in extremity trauma. *Am. J. Phys. Med. Rehabil.* **87**, 381–385 (2008).
3. E. Wang, K. Inaba, S. Byerly, D. Escamilla, J. Cho, J. Carey, M. Stevanovic, A. Ghiassi, D. Demetriades, Optimal timing for repair of peripheral nerve injuries. *J. Trauma Acute Care Surg.* **83**, 875–881 (2017).
4. L. R. Robinson, Traumatic injury to peripheral nerves. *Muscle Nerve* **23**, 863–873 (2000).
5. B. J. Pfister, T. Gordon, J. R. Loverde, A. S. Kochar, S. E. Mackinnon, D. K. Cullen, Biomedical engineering strategies for peripheral nerve repair: Surgical applications, state of the art, and future challenges. *Crit. Rev. Biomed. Eng.* **39**, 81–124 (2011).
6. A. C. Ruijs, J. B. Jaquet, S. Kalmijn, H. Giele, S. E. Hovius, Median and ulnar nerve injuries: a meta-analysis of predictors of motor and sensory recovery after modern microsurgical nerve repair. *Plast. Reconstr. Surg.* **116**, 484–494; discussion 495-486 (2005).
7. T. Gordon, N. Tyreman, M. A. Raji, The basis for diminished functional recovery after delayed peripheral nerve repair. *J. Neurosci.* **31**, 5325–5334 (2011).
8. H. M. Kaplan, P. Mishra, J. Kohn, The overwhelming use of rat models in nerve regeneration research may compromise designs of nerve guidance conduits for humans. *J. Mater. Sci. Mater. Med.* **26**, 226 (2015).
9. S. Geuna, I. Papalia, G. Ronchi, F. S. d'Alcontres, K. Natsis, N. A. Papadopulos, M. R. Colonna, The reasons for end-to-side coaptation: How does lateral axon sprouting work? *Neural Regen. Res.* **12**, 529–533 (2017).
10. S. J. Kettle, N. E. Starritt, M. A. Glasby, T. E. Hems, End-to-side nerve repair in a large animal model: How does it compare with conventional methods of nerve repair? *J. Hand Surg. Eur. Vol.* **38**, 192–202 (2013).
11. B. Mersa, D. A. Tiangco, J. K. Terzis, Efficacy of the "baby-sitter" procedure after prolonged denervation. *J. Reconstr. Microsurg.* **16**, 27–35 (2000).
12. J. Barbour, A. Yee, L. C. Kahn, S. E. Mackinnon, Supercharged end-to-side anterior interosseous to ulnar motor nerve transfer for intrinsic musculature reinnervation. *J. Hand Surg. Am.* **37**, 2150–2159 (2012).
13. J. R. Bain, Y. Hason, K. Veltri, M. Fahnestock, C. Quartly, Clinical application of sensory protection of denervated muscle. *J. Neurosurg.* **109**, 955–961 (2008).
14. J. R. Bain, K. L. Veltri, D. Chamberlain, M. Fahnestock, Improved functional recovery of denervated skeletal muscle after temporary sensory nerve innervation. *Neuroscience* **103**, 503–510 (2001).
15. E. Placheta, M. D. Wood, C. Lafontaine, E. H. Liu, J. M. Hendry, D. N. Angelov, M. Frey, T. Gordon, G. H. Borschel, Enhancement of facial nerve motoneuron regeneration through cross-face nerve grafts by adding end-to-side sensory axons. *Plast. Reconstr. Surg.* **135**, 460–471 (2015).
16. P. J. Johnson, M. D. Wood, A. M. Moore, S. E. Mackinnon, Tissue engineered constructs for peripheral nerve surgery. *Eur. Surg.* **45**, 122–135 (2013).
17. D. H. Smith, J. A. Wolf, D. F. Meaney, A new strategy to produce sustained growth of central nervous system axons: Continuous mechanical tension. *Tissue Eng.* **7**, 131–139 (2001).
18. B. J. Pfister, A. Iwata, D. F. Meaney, D. H. Smith, Extreme stretch growth of integrated axons. *J. Neurosci.* **24**, 7978–7983 (2004).
19. A. Iwata, K. D. Browne, B. J. Pfister, J. A. Gruner, D. H. Smith, Long-term survival and outgrowth of mechanically engineered nervous tissue constructs implanted into spinal cord lesions. *Tissue Eng.* **12**, 101–110 (2006).
20. B. J. Pfister, A. Iwata, A. G. Taylor, J. A. Wolf, D. F. Meaney, D. H. Smith, Development of transplantable nervous tissue constructs comprised of stretch-grown axons. *J. Neurosci. Methods* **153**, 95–103 (2006).
21. J. H. Huang, D. K. Cullen, K. D. Browne, R. Groff, J. Zhang, B. J. Pfister, E. L. Zager, D. H. Smith, Long-term survival and integration of transplanted engineered nervous tissue constructs promotes peripheral nerve regeneration. *Tissue Eng. Part A* **15**, 1677–1685 (2009).
22. J. H. Huang, E. L. Zager, J. Zhang, R. F. Groff, B. J. Pfister, A. S. Cohen, M. S. Grady, E. Maloney-Wilensky, D. H. Smith, Harvested human neurons engineered as live nervous tissue constructs: Implications for transplantation. Laboratory investigation. *J. Neurosurg.* **108**, 343–347 (2008).
23. D. H. Smith, Stretch growth of integrated axon tracts: Extremes and exploitations. *Prog. Neurobiol.* **89**, 231–239 (2009).
24. H. I. Chen, D. Jgamadze, J. Lim, K. Mensah-Brown, J. A. Wolf, J. A. Mills, D. H. Smith, Functional cortical axon tracts generated from human stem cell-derived neurons. *Tissue Eng. Part A* **25**, 736–745 (2019).
25. K. S. Katiyar, L. A. Struzyna, S. Das, D. K. Cullen, Stretch growth of motor axons in custom mechanobioreactors to generate long-projecting axonal constructs. *J. Tissue Eng. Regen. Med.* **13**, 2040–2054 (2019).
26. K. S. Katiyar, L. A. Struzyna, J. P. Morand, J. C. Burrell, B. Clements, F. A. Laimo, K. D. Browne, J. Kohn, Z. Ali, H. C. Ledebur, D. H. Smith, D. K. Cullen, Tissue engineered axon tracts serve as living scaffolds to accelerate axonal regeneration and functional recovery following peripheral nerve injury in rats. *Front. Bioeng. Biotechnol.* **8**, 492 (2020).
27. B. J. Dickson, Molecular mechanisms of axon guidance. *Science* **298**, 1959–1964 (2002).
28. T. W. Yu, C. I. Bargmann, Dynamic regulation of axon guidance. *Nat. Neurosci.* **4**, 1169–1176 (2001).
29. M. Tessier-Lavigne, C. S. Goodman, The molecular biology of axon guidance. *Science* **274**, 1123–1133 (1996).
30. S. Y. Fu, T. Gordon, Contributing factors to poor functional recovery after delayed nerve repair: Prolonged denervation. *J. Neurosci.* **15**, 3886–3895 (1995).
31. J. C. Burrell, K. D. Browne, J. L. Dutton, F. A. Laimo, S. Das, D. P. Brown, S. Roberts, D. Petrov, Z. Ali, H. C. Ledebur, J. M. Rosen, H. M. Kaplan, J. A. Wolf, D. H. Smith, H. I. Chen, D. K. Cullen, A porcine model of peripheral nerve injury enabling ultra-long regenerative distances: Surgical approach, recovery kinetics, and clinical relevance. *Neurosurgery* **87**, 833–846 (2020).
32. L. E. Kokai, D. Bourbeau, D. Weber, J. McAtee, K. G. Marra, Sustained growth factor delivery promotes axonal regeneration in long gap peripheral nerve repair. *Tissue Eng. Part A* **17**, 1263–1275 (2011).
33. N. B. Fadia, J. M. Bliley, G. A. DiBernardo, D. J. Crammond, B. K. Schilling, W. N. Sivak, A. M. Spiess, K. M. Washington, M. Waldner, H. T. Liao, I. B. James, D. M. Minteer, C. Tompkins-Rhoades, A. R. Cottrill, D. Y. Kim, R. Schweizer, D. A. Bourne, G. E. Panagis, M. Asher Schusterman II, F. M. Egro, I. K. Campwala, T. Simpson, D. J. Weber, T. Gause II, J. E. Brooker, T. Josyula, A. A. Guevara, A. J. Repko, C. M. Mahoney, K. G. Marra, Long-gap peripheral nerve repair through sustained release of a neurotrophic factor in nonhuman primates. *Sci. Transl. Med.* **12**, eaav7753 (2020).
34. Q. T. Li, P. X. Zhang, X. F. Yin, N. Han, Y. H. Kou, J. X. Deng, B. G. Jiang, Functional recovery of denervated skeletal muscle with sensory or mixed nerve protection: A pilot study. *PLOS ONE* **8**, e79746 (2013).
35. D. C. Yohn, G. B. Miles, V. F. Rafuse, R. M. Brownstone, Transplanted mouse embryonic stem-cell-derived motoneurons form functional motor units and reduce muscle atrophy. *J. Neurosci.* **28**, 12409–12418 (2008).
36. A. Hoke, T. Ho, T. O. Crawford, C. LeBel, D. Hilt, J. W. Griffin, Glial cell line-derived neurotrophic factor alters axon schwann cell units and promotes myelination in unmyelinated nerve fibers. *J. Neurosci.* **23**, 561–567 (2003).
37. L. Sheihet, O. B. Garbuzenko, J. Bushman, M. K. Gounder, T. Minko, J. Kohn, Paclitaxel in tyrosine-derived nanospheres as a potential anti-cancer agent: In vivo evaluation of toxicity and efficacy in comparison with paclitaxel in Cremophor. *Eur. J. Pharm. Sci.* **45**, 320–329 (2012).
38. J. Bushman, A. Vaughan, L. Sheihet, Z. Zhang, M. Costache, J. Kohn, Functionalized nanospheres for targeted delivery of paclitaxel. *J. Control. Release* **171**, 315–321 (2013).
39. E. Gutmann, J. Z. Young, The re-innervation of muscle after various periods of atrophy. *J. Anat.* **78**, 15–43 (1944).
40. R. Heumann, D. Lindholm, C. Bandtlow, M. Meyer, M. J. Radeke, T. P. Misko, E. Shooter, H. Thoenen, Differential regulation of mRNA encoding nerve growth factor and its receptor in rat sciatic nerve during development, degeneration, and regeneration: Role of macrophages. *Proc. Natl. Acad. Sci. U.S.A.* **84**, 8735–8739 (1987).
41. H. Thoenen, C. Bandtlow, R. Heumann, D. Lindholm, M. Meyer, H. Rohrer, Nerve growth factor: Cellular localization and regulation of synthesis. *Cell. Mol. Neurobiol.* **8**, 35–40 (1988).
42. H. Funakoshi, J. Frisen, G. Barbany, T. Timmusk, O. Zachrisson, V. M. Verge, H. Persson, Differential expression of mRNAs for neurotrophins and their receptors after axotomy of the sciatic nerve. *J. Cell Biol.* **123**, 455–465 (1993).
43. G. Raivich, M. Makwana, The making of successful axonal regeneration: Genes, molecules and signal transduction pathways. *Brain Res. Rev.* **53**, 287–311 (2007).
44. S. Sunderland, *Nerves and Nerve Injuries* (E&S Livingstone Ltd, 1968).
45. M. Saheb-Al-Zamani, Y. Yan, S. J. Farber, D. A. Hunter, P. Newton, M. D. Wood, S. A. Stewart, P. J. Johnson, S. E. Mackinnon, Limited regeneration in long acellular nerve

allografts is associated with increased Schwann cell senescence. *Exp. Neurol.* **247**, 165–177 (2013).
46. B. Rinker, J. Zoldos, R. V. Weber, J. Ko, W. Thayer, J. Greenberg, F. J. Leversedge, B. Safa, G. Buncke, Use of processed nerve allografts to repair nerve injuries greater than 25 mm in the hand. *Ann. Plast. Surg.* **78**, S292–S295 (2017).
47. N. Rbia, L. F. Bulstra, T. M. Saffari, S. E. R. Hovius, A. Y. Shin, Collagen nerve conduits and processed nerve allografts for the reconstruction of digital nerve gaps: A single-institution case series and review of the literature. *World Neurosurg.* **127**, e1176–e1184 (2019).
48. L. H. Poppler, X. Ee, L. Schellhardt, G. M. Hoben, D. Pan, D. A. Hunter, Y. Yan, A. M. Moore, A. K. Snyder-Warwick, S. A. Stewart, S. E. Mackinnon, M. D. Wood, Axonal growth arrests after an increased accumulation of schwann cells expressing senescence markers and stromal cells in acellular nerve allografts. *Tissue Eng. Part A* **22**, 949–961 (2016).
49. C. J. Phelps, C. Koike, T. D. Vaught, J. Boone, K. D. Wells, S. H. Chen, S. Ball, S. M. Specht, I. A. Polejaeva, J. A. Monahan, P. M. Jobst, S. B. Sharma, A. E. Lamborn, A. S. Garst, M. Moore, A. J. Demetris, W. A. Rudert, R. Bottino, S. Bertera, M. Trucco, T. E. Starzl, Y. Dai, D. L. Ayares, Production of alpha 1,3-galactosyltransferase-deficient pigs. *Science* **299**, 411–414 (2003).
50. K. S. Katiyar, J. C. Burrell, F. A. Laimo, K. D. Browne, J. R. Bianchi, A. Walters, D. L. Ayares, D. H. Smith, Z. S. Ali, H. C. Ledebur, D. K. Cullen, Biomanufacturing of axon-based tissue engineered nerve grafts using porcine galsafe neurons. *Tissue Eng. Part A* **27**, 1305–1320 (2021).
51. R. B. Shultz, K. S. Katiyar, F. A. Laimo, J. C. Burrell, K. D. Browne, Z. S. Ali, D. K. Cullen, Biopreservation of living tissue engineered nerve grafts. *J. Tissue Eng.* **12**, 20417314211032488 (2021).
52. B. Ekser, P. Rigotti, B. Gridelli, D. K. Cooper, Xenotransplantation of solid organs in the pig-to-primate model. *Transpl. Immunol.* **21**, 87–92 (2009).
53. S. C. Jost, V. B. Doolabh, S. E. Mackinnon, M. Lee, D. Hunter, Acceleration of peripheral nerve regeneration following FK506 administration. *Restor. Neurol. Neurosci.* **17**, 39–44 (2000).
54. S. E. Mackinnon, V. B. Doolabh, C. B. Novak, E. P. Trulock, Clinical outcome following nerve allograft transplantation. *Plast. Reconstr. Surg.* **107**, 1419–1429 (2001).
55. J. N. Jensen, M. J. Brenner, T. H. Tung, D. A. Hunter, S. E. Mackinnon, Effect of FK506 on peripheral nerve regeneration through long grafts in inbred swine. *Ann. Plast. Surg.* **54**, 420–427 (2005).
56. Y. Yan, H. H. Sun, D. A. Hunter, S. E. Mackinnon, P. J. Johnson, Efficacy of short-term FK506 administration on accelerating nerve regeneration. *Neurorehabil. Neural Repair* **26**, 570–580 (2012).
57. J. C. Maggiore, J. C. Burrell, K. D. Browne, K. S. Katiyar, F. A. Laimo, Z. Ali, H. M. Kaplan, J. M. Rosen, D. K. Cullen, Tissue engineered axon-based "living scaffolds" promote survival of spinal cord motor neurons following peripheral nerve repair. *J. Tissue Eng. Regen. Med.* **14**, 1892–1907 (2020).
58. S. E. Roberts, S. Thibaudeau, J. C. Burrell, E. L. Zager, D. K. Cullen, L. S. Levin, To reverse or not to reverse? A systematic review of autograft polarity on functional outcomes following peripheral nerve repair surgery. *Microsurgery* **37**, 169–174 (2017).

Acknowledgments: We thank D. P. Brown and N. Kameswaran for technical contributions and the National Swine Resource and Research Center and the NIH for providing embryonic pig tissue (U42 OD011140). **Funding:** Financial support was primarily provided by the U.S. Department of Defense [CDMRP/JPC8-CRMRP #W81XWH-16-1-0796 (to D.K.C.), MRMC #W81XWH-15-1-0466 (to D.K.C.), and JWMRP #W81XWH-13-207004 (to D.K.C.)], with secondary support from the Department of Veterans Affairs [Merit Review I01-BX003748 (to D.K.C.) and Career Development Awards #IK2-RX001479 (to J.A.W.) and #IK2-RX002013 (to H.I.C.)], the NIH [NRSA Graduate Research Fellowship F31-NS090746 (to K.S.K.)], and the NSF [Graduate Research Fellowship DGE-1321851 (to L.A.S.)]. Opinions, interpretations, conclusions, and recommendations are those of the author(s) and are not necessarily endorsed by the Department of Defense, the Department of Veterans Affairs, the NIH, or the NSF. **Author contributions:** D.K.C., H.C.L., and D.H.S. conceived the study and provided the experimental design. K.S.K., M.I.E., and L.A.S. fabricated the TENGs and performed in vitro characterization experiments. J.L.D., K.D.B., J.C.B., Z.S.A., and J.A.W. executed the large animal surgical paradigm. H.I.C., H.M.K., J.M.R., and E.L.Z. provided critical perspective on surgical paradigm and functional outcome measures. J.C.B., J.L.D., K.D.B., L.A.S., F.A.L., and J.A.W. performed the electrophysiological measurements. J.P.M., F.A.L., J.C.B., and K.D.B. conducted the histological assessments. D.K.C. prepared the manuscript, J.C.B. and K.S.K. assisted with figure preparation, and all other authors provided critical feedback. **Competing interests:** D.K.C., D.H.S., and H.C.L. are cofounders and K.S.K. is currently an employee of Axonova Medical LLC, which is a University of Pennsylvania spin-out company focused on the translation of advanced regenerative therapies to treat nervous system disorders. Multiple patents related to the composition, methods, and use of TENGs. D.H.S. is an inventor on several patent applications related to this work filed by the University of Pennsylvania (no. 13/156,927, filed 9 June 2011, published 8 December 2011; no. 12/194,693, filed 20 August 2008, published 11 December 2008; no. 11/429,201, filed 5 May 2006, published 28 December 2006; no. 10/496,476, priority: 4 December 2001, filed 4 December 2002, published 31 March 2005). D.H.S., D.K.C., and J.A.W. are inventors on patent applications related to this work filed by the University of Pennsylvania (no. 15/863,278, filed 5 January 2018, published 2 August 2018; no. 14/764,450, filed 31 January 2014, published 10 December 2015; PCT/US2014/014133, priority: 31 January 2013, filed 31 January 2014, published 7 August 2014). D.K.C. is an inventor on several pending patent applications related to this work filed by the University of Pennsylvania (no. 16/753,634, priority: 6 October 2017, filed 5 October 2018; published 23 July 2020). D.K.C. and J.C.B. are inventors on a pending patent application related to this work filed by the University of Pennsylvania (no. 17/776,829, filed: 13 May 2022; no. 62/937,489, priority: 19 November 2019, filed: 18 November 2020). The authors declare that they have no other competing interests. **Data and materials availability:** All data needed to evaluate the conclusions in this paper are present in the paper and/or the Supplementary Materials.

Submitted 9 September 2021
Accepted 16 September 2022
Published 4 November 2022
10.1126/sciadv.abm3291